Constraining the primordial initial mass function with stellar archaeology

Tilman Hartwig, Volker Bromm, Ralf S. Klessen, Simon C. O. Glover

Monthly Notices of the ROYAL ASTRONOMICAL SOCIETY

MNRAS **447,** 3892–3908 (2015) doi:10.1093/mnras/stu2740

Constraining the primordial initial mass function with stellar archaeology

Tilman Hartwig,[1,2,3★] Volker Bromm,[2] Ralf S. Klessen[1,4,5] and Simon C. O. Glover[1]

[1] *Universität Heidelberg, Zentrum für Astronomie, Institut für Theoretische Astrophysik, Albert-Ueberle-Str. 2, D-69120 Heidelberg, Germany*
[2] *Department of Astronomy, University of Texas, Austin, TX 78712, USA*
[3] *Institut d'Astrophysique de Paris (UMR 7095: CNRS & UPMC), 98bis Boulevard Arago, F-75014 Paris, France*
[4] *Department of Astronomy and Astrophysics, University of California, 1156 High Street, Santa Cruz, CA 95064, USA*
[5] *Kavli Institute for Particle Astrophysics and Cosmology, Stanford University, SLAC National Accelerator Laboratory, Menlo Park, CA 94025, USA*

Accepted 2014 December 22. Received 2014 December 18; in original form 2014 November 5

ABSTRACT

We present a new near-field cosmological probe of the initial mass function (IMF) of the first stars. Specifically, we constrain the lower mass limit of the Population III (Pop III) IMF with the total number of stars in large, unbiased surveys of the Milky Way. We model the early star formation history in a Milky Way-like halo with a semi-analytic approach, based on Monte Carlo sampling of dark matter merger trees, combined with a treatment of the most important feedback mechanisms. Assuming a logarithmically flat Pop III IMF and varying its low-mass limit, we derive the number of expected survivors of these first stars, using them to estimate the probability to detect any such Pop III fossil in stellar archaeological surveys. Following our analysis, the most promising region to find possible Pop III survivors is the stellar halo of the Milky Way, which is the best target for future surveys. We find that if no genuine Pop III survivor is detected in a sample size of 4×10^6 (2×10^7) halo stars with well-controlled selection effects, then we can exclude the hypothesis that the primordial IMF extended down below 0.8 $M_\odot$ at a confidence level of 68 per cent (99 per cent). With the sample size of the Hamburg/European Southern Observatory survey, we can tentatively exclude Pop III stars with masses below 0.65 $M_\odot$ with a confidence level of 95 per cent, although this is subject to significant uncertainties. To fully harness the potential of our approach, future large surveys are needed that employ uniform, unbiased selection strategies for high-resolution spectroscopic follow-up.

Key words: methods: analytical – stars: Population III – Galaxy: evolution – Galaxy: stellar content – dark ages, reionization, first stars – early Universe.

1 INTRODUCTION

The birth of the first, so-called Population III (Pop III), stars marks the transition from the 'Dark Ages' of the Universe to the complex structure we can observe today (Bromm 2013; Loeb & Furlanetto 2013; Greif 2014). These Pop III stars synthesize the first heavy elements, thus enabling the formation of subsequent generations of stars, contribute to the early reionization of the Universe, and might provide seeds for supermassive black holes (BHs; for reviews, see Barkana & Loeb 2007; Volonteri & Bellovary 2012; Karlsson, Bromm & Bland-Hawthorn 2013). Although the first stars fundamentally influenced early cosmic evolution, there are so far no direct observations of them to guide theoretical understanding. A main goal of current research is to constrain the initial mass function (IMF) for Pop III stars, because it is the key unknown in modelling their impact on cosmic history. Computer simulations predict that primordial star formation created stars with higher characteristic mass compared to the present-day case. While early simulations suggested the formation of stars with masses above 100 $M_\odot$ (Omukai & Palla 2001, 2003; Abel, Bryan & Norman 2002; Bromm, Coppi & Larson 2002), more recent work shows that the accretion discs around Pop III protostars fragment, resulting in multiple systems with masses between 10 and 100 $M_\odot$ (Stacy, Greif & Bromm 2010; Clark et al. 2011a; Greif et al. 2011b, 2012; Hosokawa et al. 2012; Hartwig et al. 2014; Hirano et al. 2014). In extreme cases, this range might even extend down to 0.1 $M_\odot$ (Dopcke et al. 2013; Stacy & Bromm 2014).

How can those theoretical predictions be empirically tested? In the absence of any *in situ* detections of individual Pop III stars, which will remain largely out of reach even for the James Webb Space Telescope, a promising alternative is stellar archaeology, the approach of scrutinizing local fossils for clues of the early Universe (reviewed in Beers & Christlieb 2005; Frebel 2010). Specifically,

★ E-mail: hartwig@iap.fr

observations of elemental abundance patterns in extremely metal poor (EMP) stars allow us to discriminate individual supernova (SN) types that have enriched the gas out of which the next generation of (Pop II) stars has formed. In principle, one has thus a handle on inferring the IMF of the first stars. Some constraints already exist. For example, current observations can be interpreted to limit the number of Pop III stars that were massive enough ($>140\,M_\odot$) to trigger hyper-energetic pair-instability supernovae (PISNe) to maximally 7 per cent of all Pop III stars (Karlsson, Johnson & Bromm 2008). However, the actual mass range and the functional shape of the primordial IMF are still highly uncertain, as they remain elusive to direct empirical study. To make progress, we here propose a novel stellar archaeological test of the Pop III IMF, targeting its crucial lower mass limit.

The fact that no Pop III survivor has been observed until now might suggest that the lower limit to the primordial IMF exceeds $M_{\rm min} = 0.8\,M_\odot$, such that all Pop III stars would have died before reaching the age of the present-day Universe. However, there are two key caveats which could greatly weaken this constraint. First, any true low-mass Pop III survivor could be 'masqueraded' through accretion of metal-enriched interstellar material from traversing the disc of the Milky Way, such that the survivor would appear as an extreme Pop II star (Frebel, Johnson & Bromm 2009). Recently, Johnson (2014) studied the metal accretion from the ISM on to Pop III stars and found that this process should lead to a unique chemical signature, because mainly gas-phase elements can be accreted, while the radiation pressure prevents dust accretion. Consequently, it is possible that some of the so-called carbon-enhanced metal-poor stars could be polluted Pop III stars, but this is still subject of an ongoing debate. Secondly, and more seriously, it is not clear that existing surveys have sampled a sufficient number of stars in either the Galactic halo or bulge to be sure that no survivor went undetected. To address the second question, we model the detailed early assembly history of the Milky Way, to obtain a realistic and statistically sound estimate of putative Pop III low-mass survivors. This in turn allows us to derive 'critical' survey sample sizes that need to be reached to effectively constrain the lower end of the primordial IMF.

We address this question by modelling the mass assembly history of a Milky Way-like halo with a semi-analytic merger tree approach, tracing the location of any low-mass Pop III stars along the tree. Including all relevant feedback mechanisms, we derive the number of possible Pop III survivors in the present-day Milky Way, together with their radial distribution.

Star formation crucially depends on the ability of the gas to cool in sufficiently short time. Since there are no metals present in the early Universe, the primordial gas cools mainly via H_2 line emission, when falling into a dark matter minihalo, predicted to be the formation site of the first stars (Haiman, Thoul & Loeb 1996a). Some metal-free haloes, however, might have been affected by ionizing radiation from neighbouring star-forming regions. The higher electron fraction left behind by these ionized regions could trigger the formation of hydrogen deuteride, which serves as an additional coolant under these conditions, enabling the primordial gas to reach lower temperatures compared to those accessible with H_2 cooling only. Although several groups have analysed this second formation mode of primordial stars, there is no agreement how it might influence the characteristic stellar masses (Johnson & Bromm 2006; Yoshida, Omukai & Hernquist 2007; Clark et al. 2011b).

Although several studies have already addressed the question whether to expect any Pop III survivors in the Milky Way and where to look for them, this topic is still under considerable debate (Karlsson et al. 2013). Due to the inside-out growth of dark matter haloes, most studies predict that first star survivors should be concentrated towards the galactic centre (e.g. White & Springel 2000; Diemand, Madau & Moore 2005; Bland-Hawthorn & Peebles 2006; Salvadori et al. 2010; Tumlinson 2010a,b), while others propose they are spread over the entire Galaxy (Scannapieco et al. 2006; Brook et al. 2007). Other studies, which use the same methodological approach, investigate the possibility that present-day galactic haloes might contain massive black holes (MBHs) which form by merging of BH remnants of the first stars (Islam, Taylor & Silk 2003, 2004a,b). These studies find that these MBHs will not be clustered towards the centre of the main halo, but rather continue to orbit within satellite subhaloes. It is therefore not clear where to focus the search for Pop III fossils, the Galactic bulge or extended halo.

There are several previous attempts to derive constraints on the primordial IMF based on stellar archaeology. Tumlinson (2006) models the chemical evolution within the hierarchical build-up of the Milky Way, to investigate the contribution of the first stars to the chemical abundance record in low-metallicity stars. He finds that existing abundance constraints do not yet allow to distinguish between different Pop III IMFs, but functions with characteristic mass of the order of a few $10\,M_\odot$, compared to the previously preferred $100\,M_\odot$, produce overall better fits to the available data. Similarly, Salvadori, Schneider & Ferrara (2007) study the stellar population history and chemical evolution of the Milky Way. By matching their predictions to the metallicity distribution function of metal-poor stars in the Galactic halo they find that Pop III stars should be more massive than $0.9\,M_\odot$. Kulkarni et al. (2013) explore the influence of Pop III stars on the abundance patterns of damped Lyman-α absorbers (DLAs), concluding that the DLA chemistry provides a sensitive probe of the primordial IMF, at least at sufficiently high redshifts. In a slightly different approach, Mapelli, Ferrara & Rea (2006) derive an upper limit on the density of Galactic intermediate-mass black holes (IMBHs), which have been proposed in their model to be the relics of Pop III stars. They compare the distribution of simulated X-ray sources with the observed one and base their conclusion on the null detection of any such source in the Galaxy. However, these IMBHs do not trace the low-mass end of the Pop III IMF. In a recent study, de Bennassuti et al. (2014) simulate the metallicity distribution function in the Galactic halo and compare this to stellar archaeology data. They find that faint SN explosions dominate the metal enrichment by the first stars, which in turn disfavours Pop III stars in excess of $140\,M_\odot$ and hence limits the upper mass end of the primordial IMF. However, none of these models has used the number of expected survivors together with the current sample sizes to directly constrain the lower mass limit of the primordial IMF.

Our paper has the following structure. In Section 2, we describe our methodology to model the hierarchical assembly of the Milky Way. In Section 3, we compare our model to empirical constraints and we present the results in Section 4. In Section 5, we test the parameter sensitivity of our model by changing several basic assumptions. We summarize our results in Section 6.

2 METHODOLOGY

Here, we present our model of structure and star formation within the Milky Way, which is also illustrated in Fig. 1. First, we discuss our implementation of hierarchical structure formation, present our model of the Milky Way, and describe our recipes for star formation and the related feedback mechanisms.

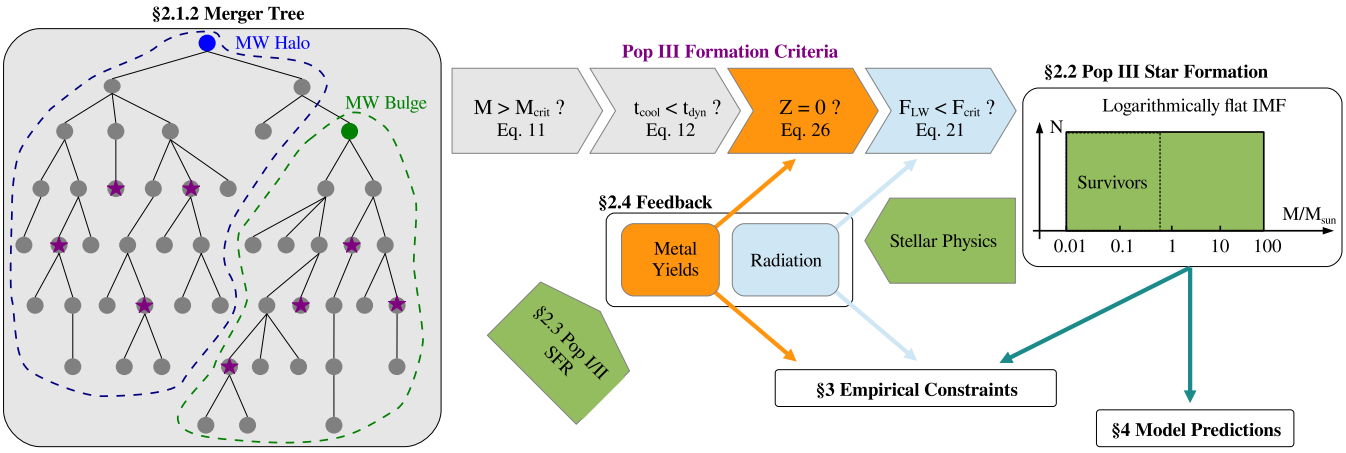

Figure 1. Road map, illustrating our model, with references to the relevant sections and equations. Based on the merger tree, we check which haloes are able to form Pop III stars. These checks include the critical mass, the absence of dynamical heating due to mergers, no pollution by metals and the strength of the LW background. We assign an individual number of Pop III stars to each successful halo and determine the influence on their environment. The contribution of Pop I/II star formation is modelled based on the analytical cosmic SFH. By comparing to existing observations, we can calibrate our model parameters. Finally, we derive a prediction for the number of Pop III survivors in the Milky Way and determine constraints on the primordial IMF.

2.1 Hierarchical structure formation

Structure formation on cosmological scales is dominated by gravity. Tiny quantum fluctuations in the very early Universe imprinted density perturbations in the dark matter component, eventually leading to the collapse of overdensities. During cosmic evolution, small haloes successively merge together to form bigger and more massive objects, giving rise to the complex hierarchy of structure in the present-day Universe. In this section, we present our methodology of determining the hierarchical mass assembly history of the Milky Way.

We assume a flat Λ cold dark matter Universe and use the cosmological parameters presented by the Planck Collaboration XVI (2014) with additional constraints from *Wilkinson Microwave Anisotropy Probe* polarization at low multipoles, high-resolution cosmic microwave background data sets, and baryonic acoustic oscillations: $H_0 = 67.77\,\mathrm{km\,s^{-1}\,Mpc^{-1}}$, $\Omega_\Lambda = 0.6914$, $\Omega_\mathrm{m} = 0.3105$, $\Omega_\mathrm{b} = 0.04825$, $n_\mathrm{s} = 0.9611$, $\sigma_8 = 0.8288$, $\tau = 0.0952$, and $Y_\mathrm{He} = 0.2477$. The dark matter power spectrum was calculated with the CAMB code by Lewis, Challinor & Lasenby (2000) for wave numbers $10^{-6}\,\mathrm{Mpc^{-1}} \leq k/h \leq 10^{6}\,\mathrm{Mpc^{-1}}$, where h is the Hubble constant in units of $100\,\mathrm{km\,s^{-1}\,Mpc^{-1}}$.

2.1.1 Extended Press–Schechter theory

Originally, Press & Schechter (1974) developed an analytical model to determine the mass assembly history of the Universe. Based on simple, generic assumptions, this 'Press–Schechter' formalism is able to predict the number density of dark matter haloes as a function of their mass and redshift with surprising accuracy. The comoving number density of haloes of mass between M and $M + \mathrm{d}M$ is given by

$$\frac{\mathrm{d}n}{\mathrm{d}M} = \sqrt{\frac{2}{\pi}}\frac{\rho_\mathrm{m}}{M}\frac{-\mathrm{d}(\ln\sigma(M))}{\mathrm{d}M}\nu_\mathrm{c}\exp(-\nu_\mathrm{c}^2/2), \tag{1}$$

where the current matter density is ρ_m, the standard deviation of the matter power spectrum is $\sigma(M)$, and $\nu_\mathrm{c} = \delta_\mathrm{c}(z)/\sigma(M)$ is the critical threshold for collapse. The time evolution of this critical overdensity for non-linear collapse is given by

$$\delta_\mathrm{c}(z) = \frac{1.686}{D(z)}, \tag{2}$$

with the linear growth factor being $D(z)$, normalized such that $D(0) = 1$. Bond et al. (1991) and Lacey & Cole (1993) improved this idea by interpreting the merger history of dark matter as a random walk in k-space, where k is the wavenumber associated with density perturbations, smoothed on a scale $2\pi/k$. This new idea also allows for the determination of merger rates and specific merger histories for individual objects.

We apply this extended Press–Schechter (EPS) approach to model more accurately the merger history of our Galaxy (Loeb 2010). The probability distribution that a mass element finds itself at z_2 in a halo of mass M_2 that was at an earlier redshift z_1 part of a halo with mass $M_1 < M_2$ is given by the conditional probability

$$\frac{\mathrm{d}P}{\mathrm{d}M_1}(M_1, z_1|M_2, z_2) = \sqrt{\frac{2}{\pi}}\frac{\delta_\mathrm{c}(z_1) - \delta_\mathrm{c}(z_2)}{[\sigma^2(M_1) - \sigma^2(M_2)]^{3/2}} \times \left|\frac{\mathrm{d}\sigma(M_1)}{\mathrm{d}M_1}\right| \exp\left(-\frac{[\delta_\mathrm{c}(z_1) - \delta_\mathrm{c}(z_2)]^2}{2[\sigma^2(M_1) - \sigma^2(M_2)]}\right). \tag{3}$$

Hence, the probability that a halo at redshift z_1 is above a mass M_0 (and will end in a halo of mass M_2 at redshift z_2) is given by $P(> M_0, z_1|M_2, z_2)$ and the corresponding number density of haloes above the critical mass is given by

$$n(> M_0) = \rho_\mathrm{m}\int_{M_0}^{\infty}\frac{\mathrm{d}P(M_1, z_1|M_2, z_2)}{\mathrm{d}M_1}\frac{\mathrm{d}M_1}{M_1}. \tag{4}$$

The original Press–Schechter formalism generally underestimates the number of low-mass haloes at high redshifts by almost an order of magnitude, compared with the results from cosmological simulations (Springel et al. 2005; Greif & Bromm 2006; Sasaki et al. 2014). However, we are explicitly interested in the exact number of these objects at high redshift. To overcome this shortcoming, we describe the mass assembly of the Milky Way with the dark matter halo merger tree algorithm by Parkinson, Cole & Helly (2008), which is originally based on the GALFORM package (Cole et al. 2000). This code constructs merger trees, following the EPS formalism (Bond et al. 1991), which reproduce the halo merger histories of the Millennium simulation (Springel et al. 2005).

2.1.2 *Merger tree*

Here, we briefly describe the original code, and discuss the latest version by Parkinson et al. (2008) used for our work. Based on the conditional probability of the EPS formalism (equation 3), one can determine the limit of $z_1 \rightarrow z_2$ and derive the instantaneous merger rate

$$\left.\frac{\mathrm{d}f}{\mathrm{d}z_1}\right|_{z_1=z_2} \mathrm{d}\ln M_1 \mathrm{d}z_1 = \sqrt{\frac{2}{\pi}} \frac{\sigma_1^2}{(\sigma_1^2-\sigma_2^2)^{3/2}} \frac{\mathrm{d}\delta_1}{\mathrm{d}z_1} \left|\frac{\mathrm{d}\ln\sigma_1}{\mathrm{d}\ln M_1}\right| \mathrm{d}\ln M_1 \mathrm{d}z_1, \quad (5)$$

where f represents the fraction of mass from haloes of mass M_2 at redshift z_2 that is contained in progenitor haloes of mass M_1 at an earlier redshift z_1 and $\delta_1 = \delta_c(z_1)$ is the critical overdensity (equation 2) at redshift z_1. Consequently, the mean number of haloes of mass M_1 into which a halo of mass M_2 splits when one takes a step $\mathrm{d}z_1$ up in redshift (and hence backwards in cosmic time) is given by

$$\frac{\mathrm{d}N}{\mathrm{d}M_1} = \frac{1}{M_1}\frac{\mathrm{d}f}{\mathrm{d}z_1}\frac{M_2}{M_1}\mathrm{d}z_1 \quad (M_1 < M_2). \quad (6)$$

For a mass resolution limit of $M_{\rm res}$, the mean number of progenitors with masses M_1 in the interval $M_{\rm res} < M_1 < M_2/2$ can be expressed as

$$P = \int_{M_{\rm res}}^{M_2/2} \frac{\mathrm{d}N}{\mathrm{d}M_1}\mathrm{d}M_1, \quad (7)$$

and the fraction of mass of the final object in progenitors below the resolution limit is given by

$$F = \int_0^{M_{\rm res}} \frac{\mathrm{d}N}{\mathrm{d}M_1}\frac{M_1}{M_2}\mathrm{d}M_1. \quad (8)$$

Note, that the quantities P and F are proportional to the redshift step $\mathrm{d}z_1$ (equation 6). For a given target mass and redshift, the GALFORM algorithm generates a corresponding binary merger tree backwards in time by choosing a redshift step $\mathrm{d}z_1$, such that $P \ll 1$, to ensure that the halo is unlikely to have more than two progenitors at the earlier redshift $z + \mathrm{d}z$. Next, it generates a uniform random number R, in the interval 0 to 1. If $R > P$, then the main halo is not split at this step. We simply reduce its mass to $M_2(1 - F)$ to account for mass accreted in unresolved haloes. Alternatively, if $R \leq P$, then we generate a random value of M_1 in the range $M_{\rm res} < M_1 < M_2/2$, consistent with the distribution given by equation (6), to produce two new haloes with masses M_1 and $M_2(1 - F) - M_1$. The same process is repeated for each new halo at successive redshift steps to build up a complete tree, which is finally stored at a limited number of output redshifts, so that each halo can have multiple progenitors at these discretized output redshifts.

The original GALFORM code systematically underpredicts the mass of the most massive progenitors for higher redshifts. Hence, we use the updated version of the code by Parkinson et al. (2008), which modifies the progenitor mass function with a perturbing function

$$\frac{\mathrm{d}N}{\mathrm{d}M_1} \rightarrow \frac{\mathrm{d}N}{\mathrm{d}M_1} G(\sigma_1/\sigma_2, \delta_2/\sigma_2) \quad (9)$$

to match the halo merger histories of the Millennium simulation (Springel et al. 2005). The best-fitting perturbing function is given by

$$G(\sigma_1/\sigma_2, \delta_2/\sigma_2) = 0.57 \left(\frac{\sigma_1}{\sigma_2}\right)^{0.38} \left(\frac{\delta_2}{\sigma_2}\right)^{-0.01}. \quad (10)$$

We have chosen this specific implementation of the merger tree, because on the one hand it provides a fast algorithm to produce merger trees with arbitrary mass resolution and on the other hand, it performs best compared to other codes. Jiang & van den Bosch (2014) recently compared four different implementations of merger trees and find the algorithm of Parkinson et al. (2008) to be the only one that yields the mass assembly history, merger rates, and the unresolved subhalo mass function in good agreement with simulations.

2.1.3 *Critical mass for baryonic collapse*

Whether the primordial gas in a halo can collapse and form stars mainly depends on its ability to cool, which in turn depends on the abundance of molecular hydrogen in the early Universe. Glover (2013) models the H_2 abundance within low density gas falling into a dark matter minihalo and derives a formula for the critical halo mass by requiring that the gas must be able to cool in less than 20 per cent of the Hubble time. Only haloes above

$$M_{\rm crit} = 6 \times 10^5 h^{-1} \left(\frac{\mu}{1.2}\right)^{-3/2} \Omega_{\rm m}^{-1/2} \left(\frac{1+z}{10}\right)^{-3/2} \mathrm{M}_\odot \quad (11)$$

fulfil this criterion, where $\mu = 1.23$ is the mean molecular weight of neutral primordial gas. The cooling condition above is only a first order approximation because gas can also be heated during halo mergers (Yoshida et al. 2003). Hence, dynamical heating from mass accretion and mergers opposes the relatively inefficient cooling by molecular hydrogen and therefore delays the formation of rapidly growing haloes (White & Rees 1978). Yoshida et al. (2003) identified the formation sites of Pop III stars and included the effect of dynamical heating. They find that molecular cooling is more efficient than the dynamical heating only if a halo with mass M has an instantaneous mass growth rate below

$$\frac{\Delta M}{\Delta z} \lesssim 3.3 \times 10^6 \,\mathrm{M}_\odot \left(\frac{M}{10^6\,\mathrm{M}_\odot}\right)^{3.9}. \quad (12)$$

Otherwise, the collapse is suppressed, or at least delayed, until the halo is massive enough to compensate this effect. We apply this criterion to our merger tree by checking for each halo that is above the critical mass whether it also fulfils this additional condition. The mass growth rate is the mass difference between the halo of interest and its most massive progenitor at the previous redshift step.

2.1.4 *Milky Way characteristics*

Due to the inside-out growth of dark matter, we expect the Galactic bulge to contain the oldest stellar relics of the Milky Way. The disc has formed later and is not relevant for our stellar archaeology approach, because there are no stars in the disc with [Fe/H] < -2.2 (Freeman & Bland-Hawthorn 2002). The ancient thick disc, which might also contain very metal poor stars, is treated as a part of the stellar halo in our study. Moreover, we do not account for dwarf satellite galaxies or globular clusters here, because we do not have the required spatial information in our merger tree model. Phrased differently, we consider metal-poor dwarf galaxies as separate entities and we focus on the smooth stellar population, which also excludes globular clusters. Although some halo stars might have been contributed from disrupted globular clusters, this can only be a small contribution to the total stellar content.

At the high redshifts of interest, the formation sites of the first stars were homogeneously distributed within the comoving volume

of the Milky Way, and some of their remnants may still be in the halo. Hence, we model the merger history of the Galactic halo and the early stellar bulge. For our model, we have to define a 'target' mass and redshift to create the corresponding mass assembly histories, where mass here represents the total mass of the halo or bulge, respectively, and the redshift marks the moment of virialization of those components. The Milky Way dark matter halo mass can be approximated by $M_{\rm halo} = (1.26 \pm 0.24) \times 10^{12}\,{\rm M}_\odot$ (McMillan 2011), which yields a comoving volume of $V_{\rm com,\,halo} = 30.3\,{\rm Mpc}^3$. The redshift however is not clearly defined, because virialization is a gradual process. Assuming mass conservation, a physical radius of 100 kpc for the stellar halo (Freeman & Bland-Hawthorn 2002), and an overdensity at virialization of $\Delta = 18\pi^2$ with respect to the mean cosmic density, we can approximate the redshift of virialization by

$$R_{\rm phys}^3 \Delta (1 + z_{\rm vir,halo})^3 = R_{\rm com}^3, \tag{13}$$

which yields $z_{\rm vir,\,halo} = 2.5$. At this redshift, we assume the mass accretion history of the Milky Way to end. For the bulge mass, we use the value of $M_{\rm bulge} = 1.8 \times 10^{10}\,{\rm M}_\odot$ (Blum 1995), which is in good agreement with other determinations, e.g. by Widrow & Dubinski (2005). Consequently, the comoving volume of the Galactic bulge is given by $V_{\rm com,\,bulge} = V_{\rm com,\,halo} M_{\rm bulge}/M_{\rm halo} = 0.43\,{\rm Mpc}^3$. Note that we assume the same cosmic background density for both components. Although the stellar density differs in bulge and halo, this mass-weighted volume is a reasonable distinction between the two regions at higher redshifts. In any case, we only need these volumina to use and determine the star formation rates per comoving volume. Moreover, our main conclusions of the analysis are rather insensitive to the choice of the bulge mass, since the Pop III survivors in the halo outnumber those in the bulge by more than an order of magnitude.

For the chemical feedback model, we need to know the physical volume of the Milky Way at any redshift, which can be determined by means of the spherical collapse model. At very high redshifts, the physical volume of the Milky Way expands with the Hubble flow until it decouples from it and undergoes gravitational collapse. The time evolution of the radius can be approximated in terms of the development angle θ by

$$\begin{aligned} r(\theta) &= A(1 - \cos\theta) \\ t(\theta) &= B(\theta - \sin\theta), \end{aligned} \tag{14}$$

where A and B are normalization parameters. For this model, virialization occurs at $\theta_{\rm vir} = 3\pi/2$ with $r_{\rm vir} = r_{\rm max}/2 = A$. Consequently, the second free parameter is given by

$$B = \frac{t_{\rm vir}}{3\pi/2 + 1}, \tag{15}$$

where $t_{\rm vir}$ is the time of virialization. We assume the virial radius of the Milky Way to be the same as its current physical radius. This approximation is valid within a factor of a few and yields reasonable results for our chemical feedback model (see Section 2.4.1).

For our modelling of the bulge, we assume that the first halo that has a mass of $M_{\rm bulge}$ will finally become the bulge, and that all Pop III stars already present in this halo will end up in the present-day bulge. The redshift at which the first halo with $M_{\rm halo} > M_{\rm bulge}$ virializes is

$$z_{\rm vir,bulge} = 9.1 \pm 0.5, \tag{16}$$

which is quite insensitive to changes in the bulge mass. A distinction between bulge and halo based on this criterion is formally only valid as long as there are no major mergers or tidal stripping events. We have checked that the last merger of haloes, with a mass ratio of 1:3 or larger, occurs before $z = 35$. However, this high redshift is a consequence of our small time steps ($\Delta z = 0.16$) and should be interpreted with caution, because e.g. the ancient thick disc could have been a merger at smaller redshifts at about this ratio.

To test this approximation, we have compared our mass-dependent definition of the bulge to the results of a three-dimensional high-resolution simulation. Using the same criterion for the bulge and tracing its most bound particles to their current positions reveals that the bulge does not end up as centrally concentrated as expected (Griffen, private communication). The final density of particles that trace the bulge has the same radial slope as the other dark matter particles. Phrased differently, most particles of the first halo with the bulge mass will not end up as the final bulge, which hence weakens our simple distinction criterion. However, this specific question on the spatial distribution of possible Pop III survivors will be subject of a subsequent study and does not affect our final conclusion.

2.2 Primordial IMF

The overall mass range of primordial star formation is not yet well known and subject to ongoing debate. Nakamura & Umemura (2002) propose a bimodal IMF with a low-mass and a high-mass star formation mode, whereas simulations of Pop III star formation predict a flat distribution of stellar masses. The possibility of disc fragmentation can lead to masses below $1\,{\rm M}_\odot$ (e.g. Clark et al. 2011a; Dopcke et al. 2013). Here, we assume a logarithmically flat IMF (Greif et al. 2011b)

$$\frac{{\rm d}N}{{\rm d}\ln M} = {\rm const.} \tag{17}$$

and explore a mass range from

$$M_{\rm min} = 0.01\,{\rm M}_\odot \tag{18}$$

to

$$M_{\rm max} = 100\,{\rm M}_\odot, \tag{19}$$

where the lower limit is close to the opacity limit for fragmentation (Rees 1976), and the upper limit is suggested by current simulations (Stacy, Greif & Bromm 2012; Hirano et al. 2014). The number of survivors is determined based on the mass, corresponding lifetime and the redshift of formation of the individual stars. Generally, Pop III stars with masses below $0.8\,{\rm M}_\odot$ might survive until today (Marigo et al. 2001), although there are individual possible survivors with masses up to $0.83\,{\rm M}_\odot$, which form at smaller redshifts.

The other key question is the amount of gas that ends up in stars per minihalo. Given the total mass of the minihalo $M_{\rm halo}$, the mass that ends in stars is given by

$$M_* = \eta_* f_{\rm LW} \frac{\Omega_{\rm b}}{\Omega_{\rm m}} M_{\rm halo}, \tag{20}$$

where the efficiency factor $f_{\rm LW}$ describes which fraction of the gas is able to collapse to cold and dense clouds under a given Lyman–Werner (LW) background and η_* defines the fraction of this gas that will finally end in stars. Note that η_* might itself depend on the halo mass, but for simplicity, we use a mean value. The fraction of cold, dense gas per minihalo under the influence of an LW background is given by (Machacek, Bryan & Abel 2001)

$$f_{\rm LW} = 0.06 \ln \left(\frac{M_{\rm halo}/{\rm M}_\odot}{1.25 \times 10^5 + 8.7 \times 10^5 F_{\rm LW}^{0.47}} \right), \tag{21}$$

where $F_{\rm LW}$ is the LW flux in units of 10^{-21} erg s^{-1} cm^{-2} Hz^{-1}. The choice for the remaining, crucial parameter of our model $\eta_* = 0.01$ will be justified in Section 3.1 by requiring to fit the optical depth to Thomson scattering measured by the Planck Collaboration XVI (2014). The more customary definition of star formation efficiency (SFE), namely the fraction of total gas mass that turns into stars, is related to our efficiency factors by $\eta_{\rm eff} = \eta_* f_{\rm LW}$.

In our model, we statistically assign a varying number of stars with specific masses to each individual halo, whereas previous studies like Trenti & Stiavelli (2009) or Kulkarni et al. (2013) average the quantities like metal yields or amount of ionizing photons over the IMF in their model. In order to do so, we randomly select stellar masses from a flat distribution between $M_{\rm min}$ and $M_{\rm max}$ in each Pop III-forming halo, so that the overall IMF follows equation (17). The assignment of stars to a halo is complete, once the total stellar mass exceeds M_*. Depending on the dark matter mass and on how far the last star overshoots this criterion, the individual systems contain different amounts of stellar mass, which reflects the stochastic nature of star formation. The assignment of stars happens instantaneously after virialization of the halo and we neglect the actual free-fall time of the gas. However, this effect might only delay the whole star formation history (SFH) in all haloes by about the same time, which is negligibly small on the considered cosmological scales.

2.3 Pop I/II star formation history

Besides an accurate treatment of Pop III star formation, we also have to model the global SFH and the contribution of Pop I and Pop II stars to the reionization and metal enrichment of the Universe. Observational constraints on the global SFH are provided by Hopkins & Beacom (2006), Li (2008), and references therein. Based on these observations, Madau & Dickinson (2014) determine the cosmic SFH

$$\Sigma_{\rm SFH}(z) = \frac{0.015(1+z)^{2.7}}{1+[(1+z)/2.9]^{5.6}}\,{\rm M}_\odot\ \ {\rm yr}^{-1}\,{\rm Mpc}^{-3}, \tag{22}$$

where they assume a Salpeter IMF (Salpeter 1955) to convert UV luminosities into instantaneous star formation rate densities. However, this formula is only valid for $z \lesssim 6$, because there are only few, indirect observational constraints for higher redshift. Hence, for higher redshifts, we use the SFH by Campisi et al. (2011), who modelled the transition of Pop III to Pop I/II star formation, based on a cosmological simulation.

2.4 Terminating primordial star formation

Not all haloes that fulfil the mass criteria (equation 11 and 12), will form Pop III stars. Feedback effects like radiation and metal enrichment influence star formation. Whereas radiation has a direct impact on star formation, chemical feedback acts indirectly, by reducing the amount of pristine gas, thus shifting the balance of star formation modes to the less efficient Pop II. A more detailed discussion of feedback effects in semi-analytical models of primordial star formation can be found, e.g. in Trenti & Stiavelli (2009), Salvadori & Ferrara (2012), and Salvadori et al. (2014). We need to know the lifetimes of stars in order to predict when a certain star explodes as an SN, thus enriching the surrounding medium, and to determine which stars actually survive until today. We interpolate between the lifetimes of non-rotating, metal-free stars provided by Marigo et al. (2001) (0.7–100 M$_\odot$), Schaerer (2002) (5–500 M$_\odot$, without mass-loss), and Ekström et al. (2008) (9–200 M$_\odot$). For masses for which several authors provide a value, we use the mean value. For rotating stars, which we analyse separately later in the paper, we use the values by Ekström et al. (2008) for the mass range 9–200 M$_\odot$. Pop III stars form predominantly between $z \simeq 15$–30, which corresponds to cosmic ages of $t = 100$–272 Myr. Given the current age of the Universe of $t_{\rm H} = 13.8$ Gyr (Planck Collaboration XVI 2014), survivors should have at least lifetimes of 13.54–13.70 Gyr. This corresponds to survival masses of $\sim$0.8 M$_\odot$.

2.4.1 *Chemical feedback*

The first stars enrich their surroundings with metals and consequently shut off the formation of subsequent Pop III stars in these regions. First, we want to focus on the metal yields and the polluted volume by a single star as a function of time. Therefore, we use a simple model for the evolution of the SN remnant (Taylor 1950; Sedov 1959; Draine 2011) to determine the time evolution of the SN-enriched volumina. The blast-wave radius as a function of time is given by

$$R(t) \propto \begin{cases} t & \text{for } t \le t_1 \\ t^{2/5} & \text{for } t_1 < t < t_2 \\ t^{2/7} & \text{for } t \ge t_2 \end{cases} \tag{23}$$

with

$$t_1 = 186\ {\rm yr}\left(\frac{M_{\rm ej}}{{\rm M}_\odot}\right)^{5/6}\left(\frac{E_{\rm SN}}{10^{51}\ {\rm erg}}\right)^{-1/2}\left(\frac{n_0}{0.1{\rm cm}^{-3}}\right)^{-1/3}$$

$$t_2 = 4.93\times10^4\ {\rm yr}\left(\frac{E_{\rm SN}}{10^{51}\ {\rm erg}}\right)^{0.22}\left(\frac{n_0}{0.1\ {\rm cm}^{-3}}\right)^{-0.55} \tag{24}$$

and

$$R(t_1) = 1.9{\rm pc}\left(\frac{M_{\rm ej}}{{\rm M}_\odot}\right)^{1/3}\left(\frac{n_0}{0.1\ {\rm cm}^{-3}}\right)^{-1/3}$$

$$R(t_2) = 23.7\ {\rm pc}\left(\frac{E_{\rm SN}}{10^{51}\ {\rm erg}}\right)^{0.29}\left(\frac{n_0}{0.1\ {\rm cm}^{-3}}\right)^{-0.42} \tag{25}$$

where $M_{\rm ej}$ is the mass of ejecta, $E_{\rm SN}$ is the explosion energy, and $n_0 \simeq 0.1{\rm cm}^{-3}$ is the number density of the surrounding medium (cf. e.g. Mesler et al. 2014). We assume an explosion energy of $E_{\rm SN} = 1.2\times10^{51}$ erg for all SNe, use the ejecta masses by Heger & Woosley (2002), and the individual metal yields by Heger & Woosley (2010). The ongoing expansion for $t \gg t_2$ should mimic the diffuse mixing of metals, which takes over for later times of the expansion.

However, the Universe was polluted simultaneously by many stars and although metal mixing is a highly complex and non-linear process, we use a simplified statistical model for the enrichment with heavy elements (following Karlsson et al. 2008) in order to distinguish whether a star forms in pristine or in previously enriched gas. Since no metal-free star is allowed to form in the previously enriched vicinity of another star, their spatial distribution is not random, but rather anticlustered. On the other hand, multiple SNe might explode in the same minihalo (Ritter et al. 2014) and the enriched volumina clearly overlap. Assuming that these two effects cancel each other out, we expect a random spatial distribution of SNe and the probability that a specific region has already been affected by k SNe follows the Poisson distribution

$$P(k, \bar{V}(t)) = {\rm e}^{-\bar{V}(t)}\frac{\bar{V}(t)^k}{k!}. \tag{26}$$

The mean value

$$\bar{V}(t) = \frac{V_{\rm enr}(t)}{V_{\rm phys}(t)} = \frac{\sum_i V_{\rm SN,i}(t)}{V_{\rm phys}(t)}, \quad (27)$$

represents the dimensionless sum of all metal-enriched volumina divided by the physical volume of the Milky Way. Note that this value can be larger than unity for later times, although there might still be regions with unpolluted gas. The probability for a star to form in pristine gas is therefore given by $P(0, \bar{V}(t))$. If for a random number $0 < r < 1$, $P(0, \bar{V}(t)) > r$, Pop III star formation is suppressed for this halo. We also track all haloes in the merger tree that have already experienced metal enrichment by a Pop III SN, and suppress subsequent primordial star formation in this halo and in all its descendants. Our simple model for metal mixing is consistent with the redshift evolution of the metal volume filling factor by Pallottini et al. (2014), who simulate cosmic metal enrichment by the first galaxies. Only for $z \lesssim 7$, our model yields lower values for the fraction of the metal polluted volume, because we do not account for the contribution of Pop I/II star formation to this volume. However, in this regime we hardly form any new Pop III stars anyway.

2.4.2 *Radiative feedback*

Pop III stars are more massive and therefore produce more high-energy photons than their present-day counterparts. Hence, they significantly contribute to reionization of the Universe with ionizing photons but also cause photodissociation of H_2 with photons in the energy range 11.18–13.6 eV, the so-called LW bands. Since the Universe is optically thin to these photons, they build up a background radiation field in the early Universe that influences primordial star formation by removing the most important coolant (Haiman, Abel & Rees 2000; Machacek et al. 2001; Wise & Abel 2007; O'Shea & Norman 2008). We use the tabulated spectra of Schaerer (2002), who provides the production rate of ionizing photons, $\dot{N}_{\rm ion}$, and the rate of photons in the LW bands, $\dot{N}_{\rm LW}$, for metal-free stars between 5 and 500 $M_\odot$. The latter is related to the flux by

$$F_{\rm LW}(z) = c\frac{h\bar{\nu}}{\Delta\nu V_{\rm com,halo}} \sum_{\rm haloes} \dot{N}_{\rm LW,i}(z) t_{*,i}, \quad (28)$$

where $\Delta\nu = 5.6 \times 10^{14}$Hz is the width of the LW bands, $h\bar{\nu} = 1.98 \times 10^{-11}$ erg is the average energy of an LW photon, $t_{*,i}$ is the lifetime of the ith star, and we sum for each redshift over all contributing Pop III stars. Here, we implicitly assume that the escape fraction of LW photons from minihaloes is 1.0, regardless of the minihalo mass or stellar mass. Generally, this escape fraction can be much smaller (Kitayama et al. 2004), but our conservative assumption tends to reduce the number of Pop III survivors by radiative feedback and hence strengthens our final conclusions. Besides LW feedback, reionization can also suppress Pop III star formation in low-mass haloes. However, this effect is only important at smaller redshifts, when hardly any Pop III stars can form anyway. Since this effect will not change our final conclusions, we do not include this feedback mechanism in the current study.

Pop III star formation likely also leads to the production of a significant soft X-ray background in the high-redshift Universe (Oh 2001; Glover & Brand 2003). The additional ionization produced by these X-rays catalyses H_2 formation, and in the absence of an LW background can exert a positive feedback on Pop III star formation (Haiman, Rees & Loeb 1996b). However, when both LW photons and X-rays are present, negative feedback from the LW photons generally dominates the positive feedback from the X-rays (Glover & Brand 2003; Machacek, Bryan & Abel 2003), and so accounting for the effects of the X-ray background would not significantly change the results of our model.

3 EMPIRICAL CONSTRAINTS

In this section, we justify our choice of parameters by comparing several model predictions to existing observations. All these empirical constraints assume that a Milky Way-like halo is representative of cosmological scales and hence that high-redshift observations reflect the state of Milky Way progenitors at earlier times. Moreover, we use these constraints to calibrate the Pop III SFE.

3.1 Optical depth to Thomson scattering

The optical depth to Thomson scattering is the most important constraint, because it can be determined fairly accurately and, together with its error bars, it yields an upper and lower limit to the star formation rate, whereas the other two empirical constraints only yield upper limits. Following Robertson et al. (2013), the optical depth is given by

$$\tau = c\sigma_{\rm T} n_{\rm H} \int_0^z {\rm d}z' f_{\rm e} Q_{\rm ion}(z')(1+z')^3 \left|\frac{{\rm d}t}{{\rm d}z'}\right|, \quad (29)$$

where z is the redshift of emission, $\sigma_{\rm T} = 0.665 \times 10^{-24}\,{\rm cm}^2$ the cross-section to Thomson scattering, $n_{\rm H}$ the comoving hydrogen number density, $Q_{\rm ion}$ the volume filling fraction of ionized regions, and $f_{\rm e}$ the number of free electrons per hydrogen nucleus (singly/doubly ionized helium) in the ionized intergalactic medium (IGM)

$$f_{\rm e} = \begin{cases} 1 + Y_{\rm p}/2X_{\rm p} & \text{at } z \leq 4 \\ 1 + Y_{\rm p}/4X_{\rm p} & \text{at } z > 4, \end{cases} \quad (30)$$

where $Y_{\rm p}$ and $X_{\rm p}$ are the primordial abundances of He and H, respectively. The time evolution of the volume filling fraction is based on

$$\frac{{\rm d}Q_{\rm ion}(z)}{{\rm d}z} = \frac{1}{n_{\rm H}}\frac{{\rm d}n_{\rm ion}(z)}{{\rm d}z} - \frac{Q_{\rm ion}(z)}{t_{\rm rec}(z)}\left|\frac{{\rm d}t}{{\rm d}z}\right|. \quad (31)$$

Here, $n_{\rm ion}$ is the comoving number density of ionizing photons, and the average recombination time in the IGM

$$t_{\rm rec} = [C_{\rm H\,II}\alpha_{\rm B}(1 + Y_{\rm p}/4X_{\rm p})n_{\rm H}(1+z)^3]^{-1}, \quad (32)$$

where $\alpha_{\rm B} = 2.6 \times 10^{-13}\,{\rm cm}^3{\rm s}^{-1}$ is the case B recombination coefficient, and $C_{\rm H\,II} = 3$ is the clumping factor (Robertson et al. 2013). For the number density of ionizing photons we have to distinguish the Pop III and Pop I/II cases.

3.1.1 *Pop I/II*

We model the SFH $\Sigma_{\rm SFH}(z)$ as described in Section 2.3, and determine the comoving number density of ionizing photons by

$$\frac{{\rm d}n_{\rm ion}(z)}{{\rm d}z} = f_{\rm esc}\eta_{\rm ion}\frac{\Sigma_{\rm SFH}(z)}{\mu m_{\rm H}}\left|\frac{{\rm d}t}{{\rm d}z}\right|, \quad (33)$$

where $f_{\rm esc} = 0.3$ is the escape fraction of ionizing photons (Greif & Bromm 2006; Robertson et al. 2013), and $\eta_{\rm ion} = 4.0 \times 10^3$ the number of ionizing photons emitted per stellar baryon (Greif & Bromm 2006). The escape fraction for the present-day Galaxy is much smaller (~6 per cent; Bland-Hawthorn & Maloney 1999) than

it was at earlier times. This is mainly due to the fact that the stellar feedback is more efficient in lower mass haloes in clearing away the gas. Since there is no unique escape fraction that is constant in space and time (Paardekooper, Khochfar & Dalla Vecchia 2013), we use this single value as an average for our simplified model. The resulting optical depth for the Pop I/II-only model is

$$\tau_{\mathrm{PopI/II}} = 0.065. \quad (34)$$

This is the baseline contribution from known stellar populations, and it is evident that hitherto undetected sources at high redshifts are needed to provide the balance.

3.1.2 *Pop III*

For the merger tree, we can directly assign the number of ionizing photons to each Pop III star based on the values by Schaerer (2002). The time-averaged escape fraction of ionizing photons in Pop III-forming haloes is $f_{\mathrm{esc,\,III}} = 0.7$ (Greif & Bromm 2006). This Pop III contribution is added to the baseline contribution by Pop I/II stars (see equation 32).

3.1.3 *Calibrating Pop III star formation efficiency*

The Planck Collaboration XVI (2014) value for the Thomson optical depth with its 1σ error is $\tau_0 = 0.0961 \pm 0.0054$, which yields a possible range of

$$0.0907 \leq \tau \leq 0.1015. \quad (35)$$

This value constrains the number of ionizing photons produced in our model, which is critically sensitive to the SFE, η_*, of Pop III stars. Consequently, we will use three different values of this efficiency for our further studies, η_{min}, η_{best}, and η_{max}, which reproduce the lowest possible, the best, and the highest possible estimate of the optical depth. The general dependence of the optical depth on the SFE and on the lower IMF mass limit can be seen in Fig. 2. The optical depth depends critically on the SFE, but hardly on the choice of M_{min}. Consequently, we can fix the SFE for our fiducial model ($M_{\mathrm{min}} = 0.01\,\mathrm{M}_{\odot}$), which yields values for η_* in the range of $\eta_{\mathrm{min}} = 0.002$ to $\eta_{\mathrm{max}} = 0.02$ with a best-fitting value of $\eta_{\mathrm{best}} = 0.01$. The corresponding optical depths as a function of redshift are displayed in Fig. 3. We emphasize that this Pop III SFE calibration is not very sensitive to the chosen value of the lower mass limit, which allows us to vary this lower limit during our analysis, without altering the SFE.

3.2 Metal enrichment

Observations of DLAs provide gas-phase metallicities at large cosmological look-back times with high precision. Hence, we use the chemical enrichment of DLAs as a constraint on the metal enrichment history of the Milky Way, under the assumption that our Galaxy went through a DLA-like phase earlier on (Kulkarni et al. 2013, 2014). Rafelski et al. (2012) provide a compilation of DLA metallicities up to redshift $z \simeq 5$, which our model should be able to reproduce. The metal enrichment is very inhomogeneous and the question of whether one can find an overdensity with a certain metallicity at a specific redshift is fundamentally a statistical one. Hence we plot, for any redshift, the mean and the maximum metallicity, which should bracket the observed metallicities. After virialization of the Milky Way ($z \simeq 2.5$), we only have one halo and consequently, mean and maximum metallicity are the same. This

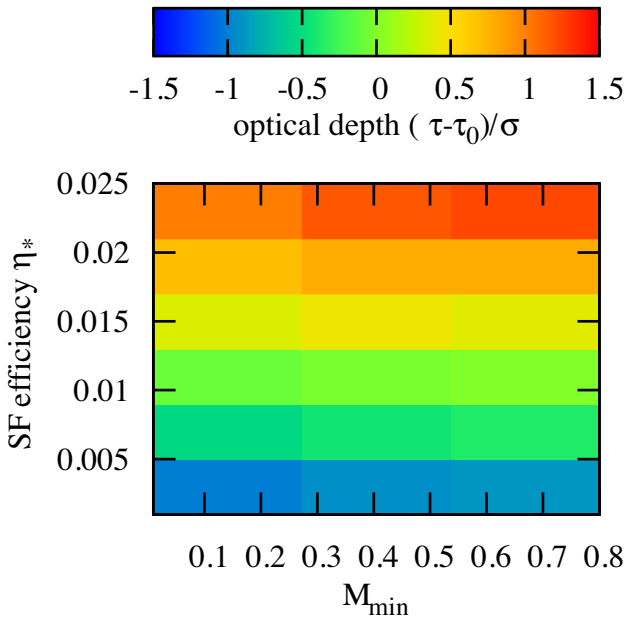

Figure 2. Optical depth minus the Planck Collaboration XVI (2014) value normalized to the 1σ error as a function of the SFE and of the lower IMF mass limit. Since ionizing photons are mainly produced by high-mass stars, the lower IMF mass limit hardly affects the optical depth. However, the optical depth crucially depends on the SFE and is therefore used to calibrate this key model parameter.

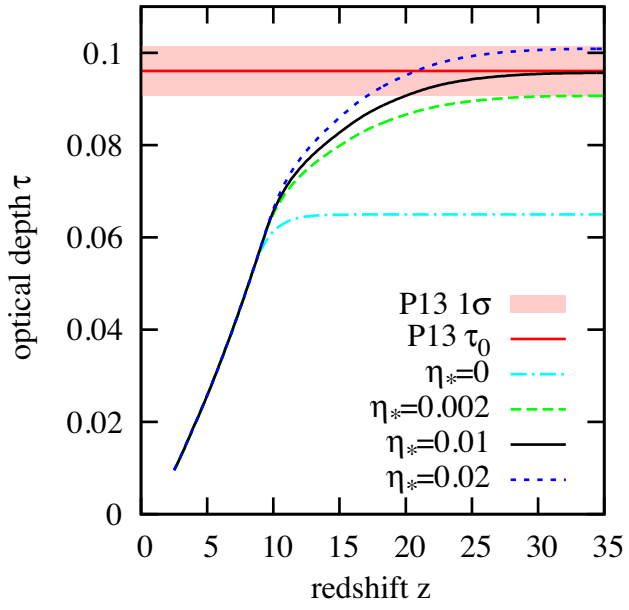

Figure 3. Optical depth as a function of redshift for different choices of the SFE η_* and comparison to the observational constraint by the Planck Collaboration XVI (2014). The contribution from Pop I/II star formation yields a baseline value of $\tau_{\mathrm{PopI/II}} = 0.065$, and the complete model results in values in accordance with the observational constraint for the three selected SFEs.

is related to our very simple estimation of the metallicity, which is just based on the mass of the halo and the mass of contained metals. However, we should keep in mind that this final target halo in our merger tree actually consists of many subhaloes, which already had higher individual metallicities at earlier times. The expectation,

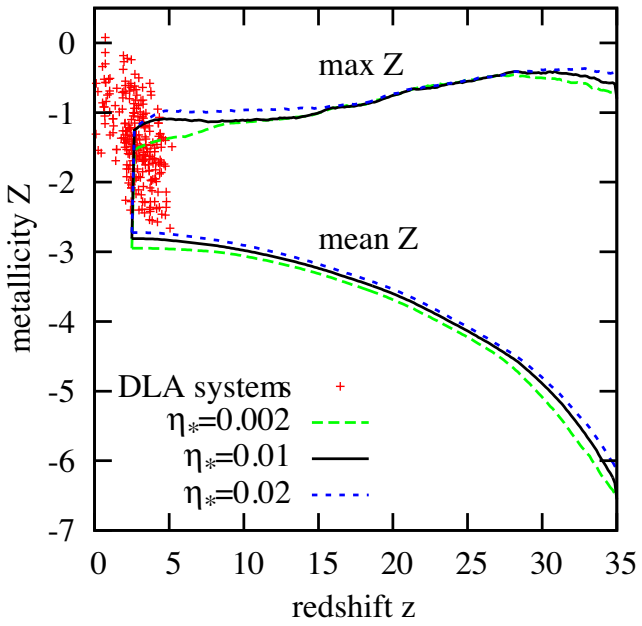

Figure 4. Mean and maximal metallicities in the proto-Milky Way-like halo, as a function of redshift, for different SFEs. The model predictions are compared to observed DLA metallicities (Rafelski et al. 2012). Evidently, we can conclude that there were already sufficiently enriched regions at high redshifts to explain the DLA metallicities, which in turn supports our metal enrichment model.

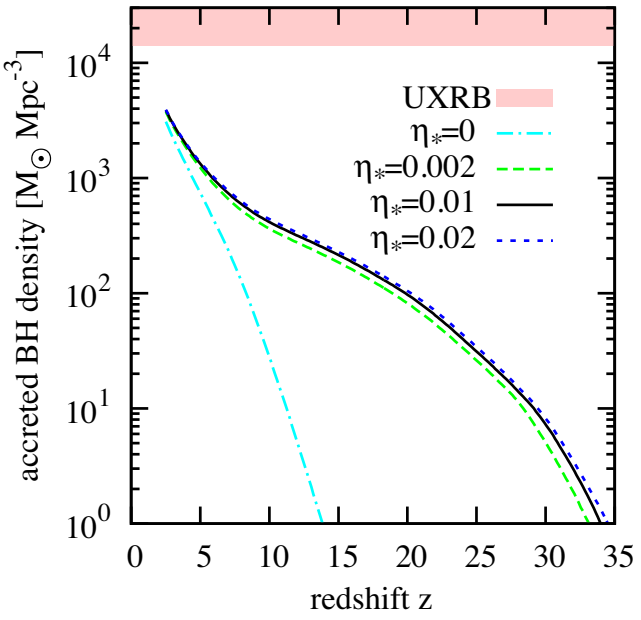

Figure 5. Mass density accreted on to BHs as a function of redshift and upper limit based on the observationally inferred UXRB. It is evident that our model does not violate this empirical constraint.

therefore, is that there must be haloes at sufficiently high redshifts that have exceeded the DLA metallicities, and finally end in the Milky Way. The metal enrichment history is illustrated in Fig. 4, which shows that this requirement is fulfilled.

3.3 Black holes and unresolved X-ray background

The formation and accretion histories of supermassive BHs are still not completely understood (Volonteri 2012), and can therefore not be used to test our model. However, measurements of the cosmic X-ray background can be used to constrain the population of high-redshift X-ray sources (Mirabel et al. 2011). The strength of the unresolved X-ray background (UXRB), yields an upper limit for the mass accreted by BHs above $z \geq 5$, which should remain below $1.4 \times 10^4\,\mathrm{M_\odot\,Mpc^{-3}}$ for $z > 5$ (Moretti et al. 2012; Salvaterra et al. 2012). In order to predict the corresponding contribution to the UXRB, we follow Jeon et al. (2014) and assume that 30 per cent of BHs evolve into a high-mass X-ray binary (Power et al. 2009), which accretes gas from the stellar companion at the Eddington rate of $2.2 \times 10^{-6}\,\mathrm{M_\odot\,yr^{-1}} (M_{\rm BH}/100\,\mathrm{M_\odot})$ for a duration of 2 Myr each. Afterwards, BHs accrete diffuse halo gas with the Bondi–Hoyle accretion rate, which varies between 10^{-14} and $10^{-6}\,\mathrm{M_\odot\,yr^{-1}}$, depending on the conditions near the BH. According to Alvarez, Wise & Abel (2009), this value is between 10^{-12} and $10^{-9}\,\mathrm{M_\odot\,yr^{-1}}$ with a mean of about $10^{-10}\,\mathrm{M_\odot\,yr^{-1}}$. This latter value also appears to be an upper limit for the accretion rates in Jeon et al. (2014). The accreted mass per Pop III-forming minihalo is therefore given by

$$M_{\rm acc,BH}(z) = \int_{z_{\rm form}}^{z} 10^{-10}\,\mathrm{M_\odot\,yr^{-1}} \frac{\mathrm{d}t}{\mathrm{d}z}\mathrm{d}z, \quad (36)$$

where $z_{\rm form}$ is the formation redshift of the BH. We estimate the baseline Pop I/II contribution from the corresponding SFH, together with the assumption that 0.8 per cent of the mass ends up in stellar mass BHs, according to a Kroupa IMF (Kroupa 2001). However, one should keep in mind that the UXRB constraint could only falsify our model in case that it were to overproduce X-rays, thus violating the empirical UXRB upper limit. As is evident from Fig. 5, our model passes this consistency check.

3.4 Hints from metal-poor stars

Our standard model assumes a logarithmically flat IMF from $M_{\rm min} = 0.01\,\mathrm{M_\odot}$ to $M_{\rm max} = 100\,\mathrm{M_\odot}$. However, in the following sections we will vary these limits and test the sensitivity of the number of Pop III survivors with respect to these parameters. For the lower IMF limit, we explore the range between the opacity limit of $0.01\,\mathrm{M_\odot}$ and the survivability threshold of $0.8\,\mathrm{M_\odot}$. If the true $M_{\rm min}$ were in excess of $0.8\,\mathrm{M_\odot}$, there would evidently exist no Pop III survivors in the local Universe. For the high-mass end of our IMF, we have to be able to create primordial stars with at least $60\,\mathrm{M_\odot}$, the Pop III progenitor mass implicated in producing the metals locked up in the most iron-poor star discovered so far (Keller et al. 2014). On the other hand, following Karlsson et al. (2008), we should limit the upper end of the IMF to $170\,\mathrm{M_\odot}$, in order to not have more than 7 per cent of Pop III stars that end as PISNe (see also Aoki et al. 2014).

4 MODEL PREDICTIONS

In this section, we present the main results of our analysis. We first discuss the Pop III SFH and related quantities, such as the build-up of LW radiation, and the different mechanisms that act to suppress Pop III star formation. Subsequently, we investigate the stellar archaeological constraints on the primordial IMF, and specifically assess the observational sample sizes required to constrain its lower mass limit.

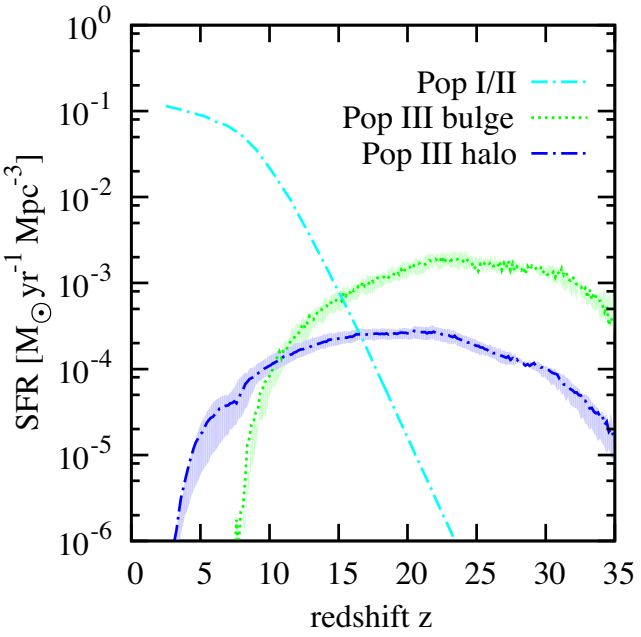

Figure 6. Star formation rate as a function of redshift for Pop III stars in the bulge and in the halo as a function of redshift. The lines represent the standard model ($\eta_* = 0.01$), whereas the shaded areas indicate the possible variations by using $\eta_* = 0.002$ and 0.02. The Pop I/II SFH is also plotted for comparison. Notice that Pop III star formation in the bulge peaks earlier and is about an order of magnitude higher than in the halo before $z \simeq 20$. Due to the much smaller volume of the bulge, the overall rate of Pop III star formation is dominated by the halo contribution.

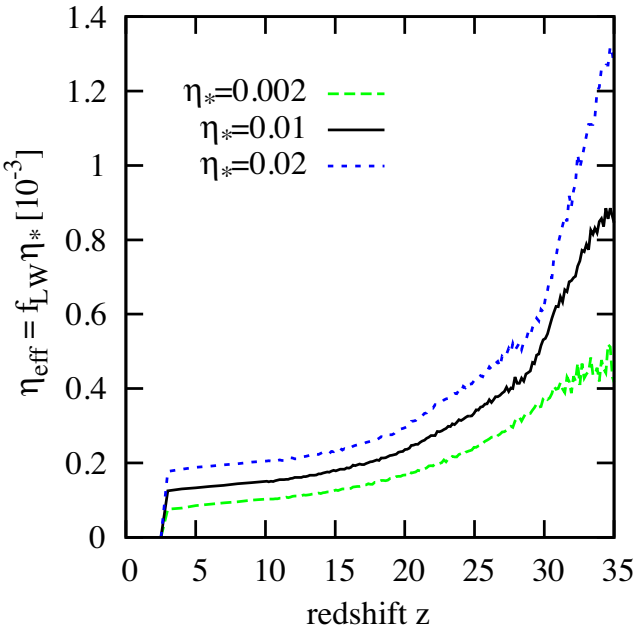

Figure 7. Overall Pop III SFE as a function of redshift. The parameter $\eta_{\rm eff}$ combines the two individual efficiencies in equation (20), and indicates which fraction of the total baryonic mass in the halo, on average, turns into Pop III stars.

4.1 History of Pop III star formation

Whereas the Pop I/II SFH is based on analytical formulas, we model Pop III star formation self-consistently with the most relevant feedback mechanisms taken into account. Moreover, our distinction between the Milky Way bulge and halo allows us to point observers to the most promising region. For each set of model parameters, we create 25 different merger tree realizations and consequently 25 slightly different merger histories of the Milky Way. The final parameters, which are presented in this section, are averaged over these merger tree realizations. The star formation rates for our fiducial model are shown in Fig. 6. The star formation rate in the bulge peaks earlier and is higher at earlier times, which is in agreement with the inside-out growth of galaxies. Following our treatment, the bulge is the first massive object that formed and therefore consists of many haloes that have virialized very early in time. Consequently, Pop III star formation in the bulge is not as influenced by suppressing feedback mechanisms as the halo. However, the comoving volume of the bulge is very small compared to the halo and therefore, the overall Pop III star formation rate is dominated by the halo contribution.

Evidently, a key parameter is the overall, halo-scale Pop III SFE, i.e. the fraction of baryonic matter that turns into Pop III stars in each dark matter host halo. This parameter is determined by the ability of the gas to cool, and therefore depends on its chemical composition and the presence of external radiation backgrounds. The resulting effective (overall) SFEs in our model are shown in Fig. 7. The decrease in SFE from 10^{-3} to 10^{-4} between $z \simeq 35$ and $\simeq 10$ is mainly driven by the increasing LW background (see Fig. 8), such that the associated photodissociation of H_2 limits the ability of the primordial gas to cool.

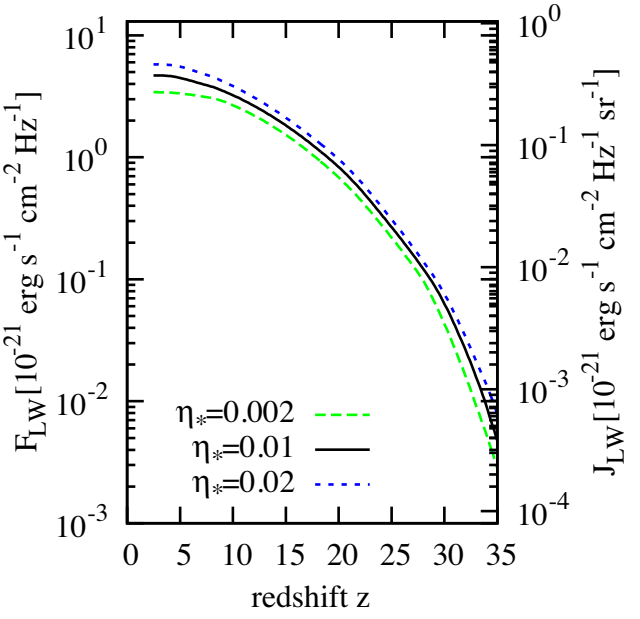

Figure 8. Average background flux of LW photons as a function of redshift. Our model prediction is consistent with the results by Johnson, Greif & Bromm (2008).

A related question concerns the fragmentation and the number of primordial stars per halo. We assign individual stars to each Pop III-forming halo, until we reach the desired total stellar mass in this halo. The corresponding number of stars per halo as a function of redshift can be seen in Fig. 9. In our model, only some systems contain one Pop III star, whereas the majority of the systems contain binary or higher multiple systems. Some rare systems host even up to 19 Pop III stars. These multiplicities are not based on a

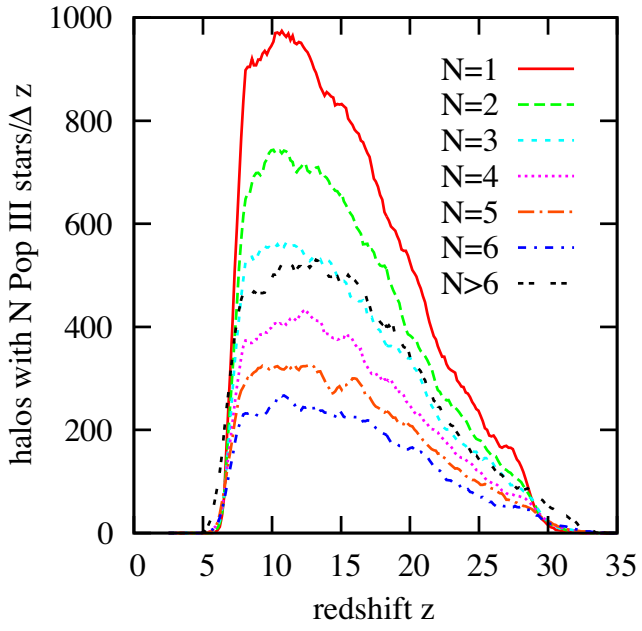

Figure 9. Number of Pop III stars per minihalo for our standard model. At any redshift, this plot illustrates how many new haloes form with N Pop III stars per unit redshift bin. Although we use a simple probabilistic IMF sampling, this approach reproduces the results of numerical simulations that most of the primordial stars form in higher multiple systems.

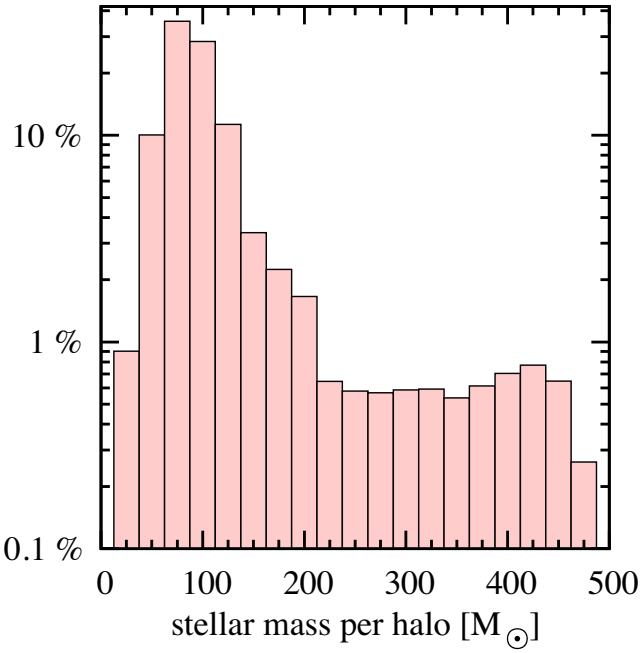

Figure 10. Distribution of the stellar mass per halo. Most of the haloes have a stellar mass content of $\sim$100 $M_\odot$ and the broad distribution from $\sim$25 to $\sim$500 $M_\odot$ reflects the stochastic nature of Pop III star formation and disc fragmentation.

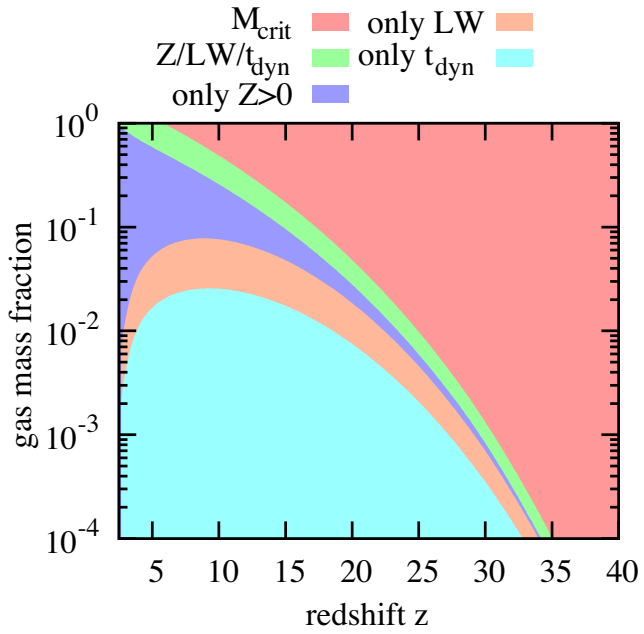

Figure 11. Relevance of different feedback and suppression mechanisms for Pop III star formation. At any redshift, this plot illustrates the dominant suppression effects, quantified by their respective gas mass fractions. $M_{\rm crit}$ reflects gas that is not part of sufficiently massive haloes. The green area indicates the gas that does not form Pop III stars because of suppression by several mechanisms, whereas the purple, magenta, and blue areas represent gas that cannot form Pop III stars only because of previous metal enrichment, too strong an LW flux, or dynamical heating, respectively. Keeping in mind the logarithmical scaling, it can be seen that the only relevant suppression mechanisms are metal enrichment at smaller redshifts and the critical mass criterion earlier on.

detailed three-dimensional disc fragmentation simulation, but are rather based on a probabilistic assignment. Phrased differently, we do not mimic mergers or ejections of primordial stars, but assign the final number of stars to the system. Although the outcome agrees with simulations, this distribution of multiplicities is not physically motivated. The associated stellar mass per halo can be seen in Fig. 10. Following our recipe of Pop III star formation, we have a broad range of stellar masses per halo from $\sim$25 to $\sim$500 $M_\odot$ with a mean around $\sim$100 $M_\odot$. This distribution complies with the expectation from numerical simulations of disc fragmentation in primordial gas clouds.

Regarding the termination of Pop III star formation, we are interested in the different feedback mechanisms and their individual importance. In our model, dark matter haloes have to fulfil four criteria in order to form Pop III stars: they have to be massive enough, should not be affected by dynamical heating due to mergers, should not have been polluted by metals, and should not experience too strong an LW background. In our merger-tree algorithm, we do not resolve haloes below 6×10^4 $M_\odot$, and therefore cannot assess the detailed physics of suppressing star formation inside these haloes. However, for all other haloes, we can explicitly identify whether one effect dominates, or whether several criteria suppress star formation simultaneously. The time-dependent relevance of different suppression mechanisms is shown in Fig. 11. The critical mass is obviously the dominant suppression mechanism most of the time. Only at smaller redshifts, other feedback mechanisms become important. Whereas there are hardly any haloes in which Pop III star formation is suppressed only because of the LW background or dynamical heating, there is quite a number of haloes that cannot form Pop III stars because of metal enrichment or a combination of these feedback mechanisms.

4.2 Stellar archaeology

We can constrain the lower mass limit of the primordial IMF from the fact that we have not observed any Pop III star so far. Moreover, we can wield this null result into an accurate probe of $M_{\rm min}$ by considering the current survey sizes of EMP stars. The basic idea here is that the probability for the detection of a Pop III survivor increases with decreasing $M_{\rm min}$. The ongoing efforts by stellar archaeologists thus provide ever improving empirical upper limits on this survival probability ($P_{\rm surv} < 1/N_{\rm sample}$). The exciting prospect then arises that even the non-detection of a Pop III survivor can constrain the primordial IMF at a level of precision that is otherwise completely out of range. In the following, we discuss this IMF probe in detail.

4.2.1 Current sample size

Our statistical analysis is based on a combinatorial argument. Hence, we need to know the current sample size, $N_{\rm o}$, of randomly chosen stars, from which candidates have been photometrically selected for follow-up spectroscopic measurement of their metallicity. To detect a primordial star, it has to show no sign of metal lines of any kind in its stellar spectrum. The most prominent lines used to determine metallicity are the Ca II, K, or Fe I lines (Caffau et al. 2011, 2013). The Fe I line by itself is not a good indicator, as we know of at least one star which appears to be entirely iron deficient, but which despite this has a carbon abundance of [C/H] ~ -2.5, and which is therefore not a Pop III star (Keller et al. 2014). To exclude the primordial composition, we need high-resolution spectra with spectral resolution $R > 20\,000$ and a signal-to-noise ratio of S/N > 50, which are currently available for $\sim$1000 halo stars and which will serve as a conservative lower value. However, the Hamburg/European Southern Observatory (ESO) survey has observed $\sim 4 \times 10^6$ individual sources (Christlieb, private communication), photometrically selected metal-poor candidates and spectroscopically measured the actual metallicity of a smaller subset. For our further analysis, we are interested in the number of randomly selected halo stars. Since the original sample of point sources contained also quasars, oversaturated stars or disc stars, the actual number is somewhat lower and we use $N_{\rm o} = 10^6$ as a rough upper limit:

$$10^3 \lesssim N_{\rm o,h} \lesssim 10^6. \tag{37}$$

However, one should keep in mind that the selection criteria for follow-up spectroscopy might have rejected a metal-free star (Christlieb et al. 2008).

For the Milky Way bulge, the number of observed stars is much smaller. There are observations of 100 EMP stars (García Pérez et al. 2013), which were selected from a slightly bigger sample and will serve as a lower estimate. The abundances and radial velocity galactic origins survey, however, obtained spectra for $N_{\rm o} = 28\,000$ stars at a spectral resolution of $R = 11\,000$, which will serve as an upper limit for the bulge (Ness et al. 2013). Consequently, the current sample size for the bulge is in the range

$$10^2 \lesssim N_{\rm o,b} \lesssim 2.8 \times 10^4. \tag{38}$$

The actual numbers of the current sample sizes for bulge and halo do not directly enter our statistical model, but should give a rough idea of the effectiveness of continuing observations in these regions.

4.2.2 Statistical description

Since the statistical method is the same for bulge and halo, we will derive it for an arbitrary set of $N_{\rm t}$ stars in total with $N_{\rm o}$ observed stars and $N_{\rm s}$ expected survivors. Note, that $N_{\rm o}$ is treated as a free parameter, reflecting the increasing sample sizes of upcoming surveys. The total number of different realizations, where we observe $N_{\rm o}$ out of $N_{\rm t}$ stars is given by

$$N_{\rm tot} = \binom{N_{\rm t}}{N_{\rm o}}. \tag{39}$$

The number of different realizations, where we observe $N_{\rm o}$ out of $N_{\rm t}$ stars, but do not observe any Pop III survivor is given by

$$N_{\rm not} = \binom{N_{\rm t} - N_{\rm s}}{N_{\rm o}}. \tag{40}$$

The probability that we have missed all expected Pop III survivors in the observed sample is therefore given by

$$p_0 = \frac{N_{\rm not}}{N_{\rm tot}} = \frac{(N_{\rm t} - N_{\rm s})!(N_{\rm t} - N_{\rm o})!}{N_{\rm t}!(N_{\rm t} - N_{\rm s} - N_{\rm o})!}. \tag{41}$$

In the Milky Way, the values of $N_{\rm t}$, $N_{\rm s}$, and $N_{\rm o}$ are too high to calculate the factorial. Hence, we use Stirling's formula to simplify matters

$$\begin{aligned}\ln p_0 = {} & (N_{\rm t} - N_{\rm s}) \log(N_{\rm t} - N_{\rm s}) + (N_{\rm t} - N_{\rm o}) \log(N_{\rm t} - N_{\rm o}) \\ & - N_{\rm t} \log(N_{\rm t}) - (N_{\rm t} - N_{\rm o} - N_{\rm s}) \log(N_{\rm t} - N_{\rm o} - N_{\rm s}).\end{aligned} \tag{42}$$

Phrased differently, $p = 1 - p_0$ describes the probability that the current sample size is representative and we have no Pop III survivor in the Milky Way.

Based on the lower mass limit for the primordial IMF $M_{\rm min}$, our semi-analytic model predicts the number of Pop III survivors. Using equation (42), we can now determine the critical sample size to exclude Pop III stars with masses below $M_{\rm min}$ for three different reliability thresholds. This statistical prescription is valid, as long as the sample is a random, unbiased selection of stars and all stars have the same probability of being observed. For previous surveys, the latter assumption generally breaks down for stellar masses below $\sim 0.6\,{\rm M}_\odot$, because these stars are generally to faint for direct observation (Frebel, private communication). However, this threshold is also a moving target, which might decrease with upcoming surveys.

4.2.3 Prediction of lower IMF limit

We now proceed to the core of our argument, deriving the sample sizes required to effectively constrain the lower mass limit of Pop III. An important parameter for our analysis is the total number of stars in the Milky Way bulge and halo. For a characteristic mass of a star of $0.38\,{\rm M}_\odot$ (Kroupa 2001), total stellar masses of about $10^9\,{\rm M}_\odot$ for the metal-poor halo and $2 \times 10^{10}\,{\rm M}_\odot$ for the bulge we expect $N_{\rm t,\,h} \simeq 2.5 \times 10^9$ stars in the halo and $N_{\rm t,\,b} \simeq 5.5 \times 10^{10}$ stars in the bulge. Although these values are crucial for our conclusion, we can only provide an order of magnitude estimate. To illustrate this uncertainty, we assume that both numbers are subject to an error of 25 per cent. The resulting constraints on the lower IMF limit as a function of the sample size can be seen in Fig. 12. There are several important conclusions that we can draw from this plot. The sample size needed for constraining $M_{\rm min}$ is more than two orders of magnitude higher for the Milky Way bulge than for the halo. Consequently, observations in the halo are much more promising for constraining the lower mass IMF limit, especially because the current sample size is already higher for the halo and because observations in the bulge are hindered by dust extinction. For an optimistic reading of the sample size of the Hamburg/ESO survey and a conservative

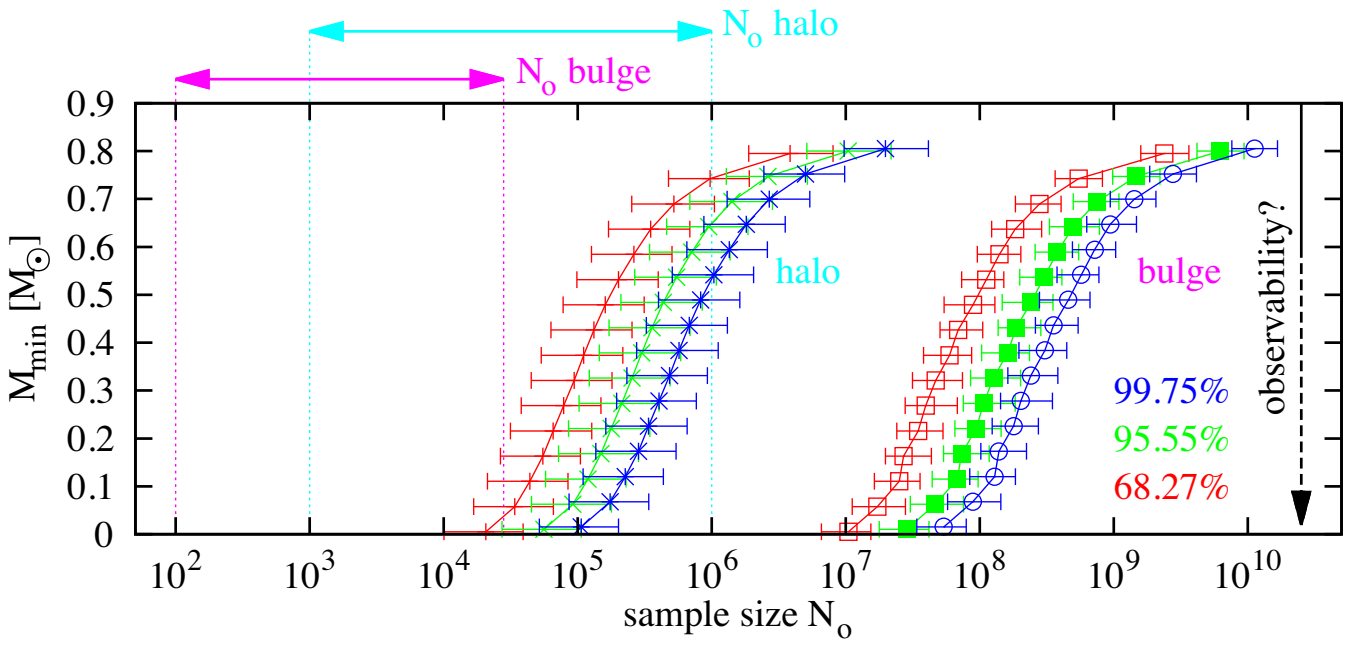

Figure 12. Constraints on the lower IMF limit as a function of the sample size, whereas the different lines represent the confidence levels of 68.27, 95.55, and 99.73 per cent. The vertical dashed lines in magenta and light blue indicate the current sample sizes, respectively, the number of stars that have already been observed and that are certainly not Pop III stars. The vertical arrow on the right illustrates the reduced observation probability for stars below $\sim 0.6\,M_\odot$. However, since we model star formation separately for every value of $M_{\rm min}$, values above the observability threshold are not affected by the reduced observability for smaller stellar masses. For the bulge, we have to observe a much higher number of stars to find a constraint on $M_{\rm min}$, compared to the halo. Furthermore, it is noticeable that we are already in the interesting regime for the halo and we need sample sizes of 4×10^6, 1×10^7, and 2×10^7 to exclude any Pop III survivors with a confidence level of 68.27, 95.55, and 99.73 per cent, respectively. The error bars include the uncertainty in the SFE, in the total number of stars $N_{\rm t}$ and the statistical scatter between several merger tree realizations.

treatment of the error bars, we could already exclude the existence of any Pop III stars with less than $\sim 0.65\,M_\odot$ with a certainty of 95 per cent. However, for a more restrictive reading (corresponding to $\sim 10^3$ halo stars surveyed at sufficiently high quality), no constraints could yet be placed on the Pop III IMF. In order to exclude any Pop III survivors with a certainty of 99 per cent, a critical sample size of $\sim 2 \times 10^7$ halo stars has to be achieved, which should be well within reach of upcoming stellar archaeological campaigns. However, designing a well-considered observing plan is out of the scope of this work. A basic assumption of this statistical analysis is that all stars have the same probability of being observed. Once this assumption breaks down, we might have to correct for the reduced observation probability. However, any conclusions drawn from the mass range above $\sim 0.65\,M_\odot$ is not affected by this caveat.

5 CAVEATS AND PARAMETER SENSITIVITY

Although we include the most relevant feedback mechanisms and calibrate our model against empirical constraints, there are several approximations and limitations that introduce uncertainties to our results. In this section, we investigate these caveats and address the question of how sensitive our model is to the specific choice of parameters. We begin by discussing some of the processes that are not included in our current approach in Section 5.1. It is fair to say that the numerical calculations of Pop III star formation that aim at resolving individual objects are still in their infancy and leave room for large uncertainties with respect to stellar multiplicity and rotation as well as to the IMF. We assess the influence of these uncertainties in Sections 5.2 and 5.3, respectively. Another key factor that enters our model is the cosmic reionization history, as modelled by the escape fraction of ionizing radiation. The uncertainties in this parameter are explored in Section 5.4. We focus our discussion on the number of expected Pop III survivors as our primary prediction, and provide the corresponding plots in Fig. 13.

5.1 Neglected effects

There are a number of physical processes and effects that are not yet included in our model. The first simplification is that our approach is a purely statistical one. We have no information about the exact spatial location of dark matter haloes and the distance to their neighbours. For this reason, we can address the question of how feedback influences other haloes only in a probabilistic and rather idealized fashion. By the same token, we can determine whether a high-redshift halo will become part of the Milky Way halo or the bulge in a statistical sense only.

Furthermore, we also neglect the effects of streaming velocities (Tseliakhovich & Hirata 2010) on the dynamics of primordial haloes and on their ability to form stars. This effect may lead to a delayed onset of Pop III star formation, possibly occurring in haloes of somewhat larger masses than we assume here (e.g. Greif et al. 2011a; Maio, Koopmans & Ciardi 2011; Stacy, Bromm & Loeb 2011). However, we note that in the model of Tseliakhovich, Barkana & Hirata (2011), the critical mass for collapse in a typical region is increased by only one order of magnitude and hence remains smaller than our $M_{\rm crit}$ at all redshifts $z < 40$ (Glover 2013). It is therefore plausible that properly accounting for the effects of streaming velocities would not make a major difference to the results of our model. We also do not include magnetic fields or the potential effects of dark matter annihilation when calculating the

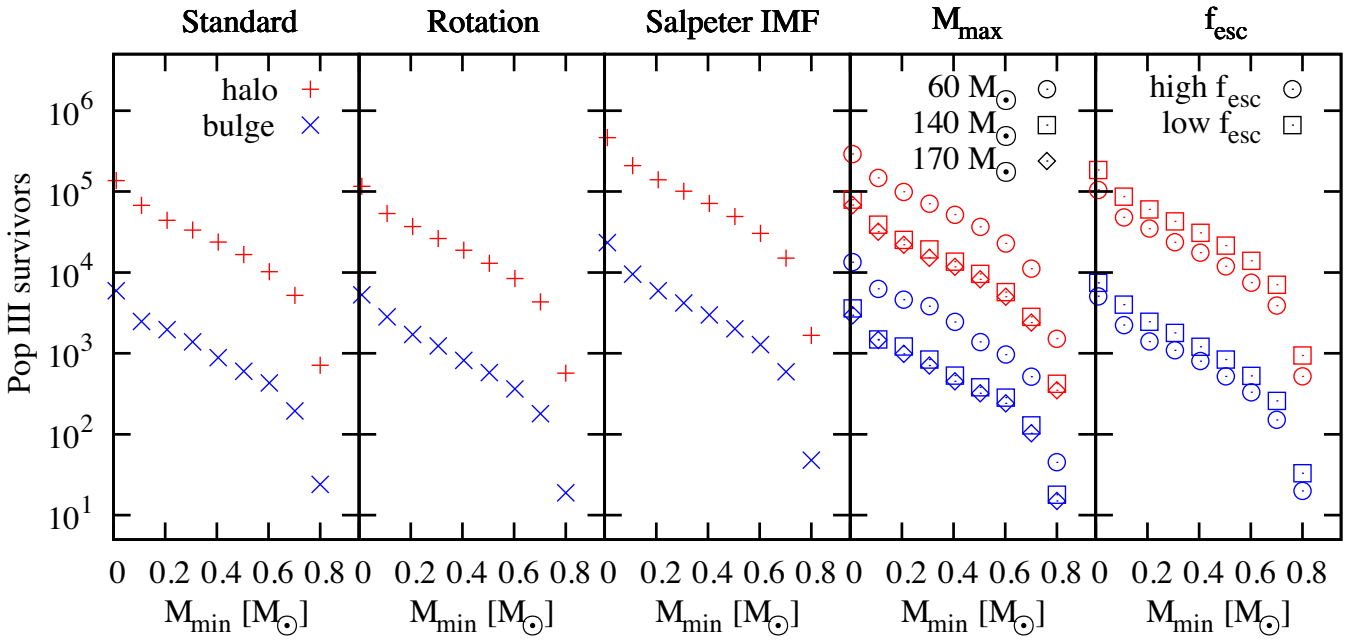

Figure 13. Expected number of Pop III survivors as a function of the lower IMF limit for different assumptions. The standard model assumes non-rotating Pop III stars with a logarithmically flat IMF, masses up to 100 $M_\odot$, and escape fractions of $f_{\rm esc,\,III} = 0.7$ and $f_{\rm esc} = 0.3$. The assumption of rotating Pop III stars increases the stellar lifetimes, hence the production of ionizing photons. Consequently, the SFE and the number of survivors is slightly smaller. For a Salpeter IMF, the SFE has to be considerably higher and we expect about an order of magnitude more survivors. The upper mass limit of the primordial IMF is a crucial parameter and, especially for values $<100\,M_\odot$, it has a significant influence on the number of survivors, because it determines the gas mass that is left over for possible survivors. The escape fraction for ionizing photons is very uncertain, but even a large change in this parameter hardly influences the number of Pop III survivors. This parameter study shows that most uncertainties might yield even more Pop III survivors, which in turn strengthens our final conclusions.

stability of haloes against gravitational collapse. It is likely that the gas in primordial haloes was substantially magnetized, because any pre-existing field was easily amplified to dynamically significant levels by the small-scale turbulent dynamo. This process converts parts of the kinetic energy of the halo gas into magnetic energy (Schleicher, Banerjee & Klessen 2008; Schleicher et al. 2010; Sur et al. 2010; Schober et al. 2012). Also, if dark matter particles are self-annihilating, then the additional heat generated by this process could influence the star formation process (e.g. Freese et al. 2008; Iocco 2008; Schleicher et al. 2009a; Schleicher, Banerjee & Klessen 2009b; Spolyar et al. 2009; Smith et al. 2012). Both effects increase the minimum mass for collapse. Moreover, our star formation criteria are just a first approximation. The critical mass threshold alone might not be sufficient to decide whether a dark matter halo can collapse to form primordial stars (Sasaki, private communication). Similar holds for the transition from Pop III to Pop I/II star formation. A more sophisticated approach in the future should include a more detailed treatment of metal mixing and a better description of ionizing radiation.

We also mention that our approach does not account for the possibility that Pop III survivors might be polluted with metals after they have formed, either within the original halo or later on, once they have become part of the Galaxy (see, e.g. Frebel et al. 2009; Johnson 2014). The recent detection of an extremely iron-poor Pop II star (Keller et al. 2014) suggests that pollution does not significantly affect the observed metallicities of all of the currently known EMP stars, but the fraction that are significantly affected has yet to be properly quantified. Most ancient open clusters show chemical homogeneity (Bland-Hawthorn, Krumholz & Freeman 2010; Friel et al. 2014), which decreases the possibility that single stars are polluted. However, it is generally possible that all cluster stars have the same surface contamination. For the purposes of our current study, we assume that the effects of pollution are either negligible or can be identified and corrected for.

5.2 Rotation

So far, our model is based on the assumption of non-rotating Pop III stars. However, Ekström et al. (2008) have shown, together with other groups, that rotation can significantly influence the evolution of metal-free stars, and Stacy et al. (2013) illustrate the possibility of rapidly rotating Pop III protostars. The rotationally induced mixing increases the mass of the He cores at the end of the evolution, which in turn changes the final fates of the Pop III stars. Generally, rotation leads to longer lifetimes and higher metal yields. Hence, we expect stronger feedback effects via metal pollution, LW radiation, and ionizing photons. Furthermore, the mass ranges of the final fates of primordial stars slightly change. To study the effect of rotation on the number of Pop III survivors, we assume all Pop III stars to be strongly rotating, with the corresponding stellar lifetimes and ejecta masses (Ekström et al. 2008). For the mass ranges of primordial stars that end as BHs, we use the He-core masses at the pre-SN stage, interpolate between them, and compare to the results of Heger & Woosley (2002). This yields BH remnants for initial masses of Pop III stars in the range ∼25–75 $M_\odot$ and above 240 $M_\odot$. Assuming the same production rate of ionizing photons, the SFE has to be smaller to compensate for the longer lifetimes of the stars. The best-fitting value of $\eta_{*,\rm rot} = 0.004$ yields an optical depth of $\tau = 0.0957$. The mass accreted on to BHs is still below the limit given by the UXBG and the mean and maximal metallicity are slightly higher compared to the values in Fig. 4, but are still in compliance with the observed DLAs. The corresponding numbers

of expected survivors can be seen in Fig. 13. A proper treatment of rotation might also account for the different stellar spectra of rotating stars and include a distribution of rotation velocities, but from this first analysis we already see that the differences in the number of survivors are not huge. Consequently, the question of whether Pop III stars are rapidly rotating or not, has no significant influence of the results of this study.

5.3 IMF dependence

The actual shape of the primordial IMF is the largest unknown in our model. While we explicitly vary and try to constrain the lower mass end in this paper, the actual slope and the high-mass end are still uncertain. Here, we wish to study the sensitivity of our results to changes in the IMF high-mass end and its slope. Whereas a logarithmically flat IMF seems to agree best with current simulations (Greif et al. 2011b; Dopcke et al. 2013; Hirano et al. 2014), we also want to test the assumption of a Salpeter IMF with a slope of $\alpha = -1.35$ (Salpeter 1955). To match the optical depth criterion, we have to use an SFE of $\eta_* = 0.02$ in this case. The results in Fig. 13 show clearly that a Salpeter IMF yields a higher number of Pop III survivors, because almost no Pop III stars might be massive enough to produce sufficiently many ionizing photons to reproduce the optical depth. We note, however, that the numerical simulations do not favour such a bottom-heavy IMF and a higher number of Pop III survivors, caused by a steeper IMF, might even strengthen our conclusion.

The high-mass end of the IMF limits the amount of gas that is left for low-mass stars and possible survivors. The associated SFEs are $\eta_*(60\,\mathrm{M}_\odot) = 0.03$, $\eta_*(140\,\mathrm{M}_\odot) = 10^{-3}$, and $\eta_*(170\,\mathrm{M}_\odot) = 10^{-4}$ to match the optical depth constraint. Especially for masses $<100\,\mathrm{M}_\odot$, the number of survivors depends crucially on this parameter. Specifically, $M_{\mathrm{max}} < 100\,\mathrm{M}_\odot$ might yield more possible survivors, thus strengthening our argument, whereas $100\,\mathrm{M}_\odot < M_{\mathrm{max}} < 170\,\mathrm{M}_\odot$ does not significantly reduce the number of survivors. This simple analysis shows that the value of $M_{\mathrm{max}} = 100\,\mathrm{M}_\odot$ for our fiducial model is not only in good agreement with simulations, but also yields a reasonable lower limit on the number of expected Pop III survivors and hence supports our final conclusion.

5.4 Reionization history

The escape fraction of ionizing radiation is very uncertain and might vary with redshift and halo mass. Here, we study the dependence of the escape fraction on our model predictions. Therefore, we vary the fiducial escape fractions of $f_{\mathrm{esc,\,III}} = 0.7$ and $f_{\mathrm{esc}} = 0.3$ to $f_{\mathrm{esc,\,III}} = 0.6$ and $f_{\mathrm{esc}} = 0.2$, and to $f_{\mathrm{esc,\,III}} = 0.8$ and $f_{\mathrm{esc}} = 0.4$, adjusting the SFE accordingly ($\eta_* = 0.025$ for low escape fractions and $\eta_* = 0.002$ for high escape fractions) to reproduce the optical depth and compare the predicted number of survivors for each case. The reionization history can be seen in Fig. 14 for our standard model, and for different SFEs. Even for these different escape fractions, the expected numbers of Pop III survivors do not change significantly. Consequently, the predictions by our model are not very sensitive on the exact reionization history.

6 SUMMARY AND CONCLUSIONS

We have used a semi-analytical model to determine the Pop III SFH in a Milky Way-like halo. This model, which was based on a Monte Carlo sampling of merger trees, contained radiative and chemical feedback to self-consistently suppress Pop III star formation at smaller redshifts. We were able to reproduce a suite of independent observations like the optical depth to Thomson scattering and the metal enrichment history. Primordial stars with masses below $\sim 0.8\,\mathrm{M}_\odot$ might have survived until today and should be observable in large surveys. Comparing the expected number of Pop III survivors in our model to estimates of current survey sizes enables us to constrain the lower mass IMF limit to $0.65\,\mathrm{M}_\odot$ with a confidence of 95 per cent. For non-detections to exclude any Pop III survivor, and hence set $M_{\mathrm{min}} \geq 0.8\,\mathrm{M}_\odot$, the future surveys need to include at least $\sim 2 \times 10^7$ halo stars. In order to draw the same conclusions from observations of stars in the Milky Way bulge, we have to observe $\sim 10^3$ times more stars. This comes from the fact that there are generally more stars in the bulge and the absolute number of Pop III survivors is smaller there. In addition, the determination of stellar metallicities is hindered by dust distinction and consequently the current sample sizes for bulge stars are smaller, compared to those of the Milky Way halo.

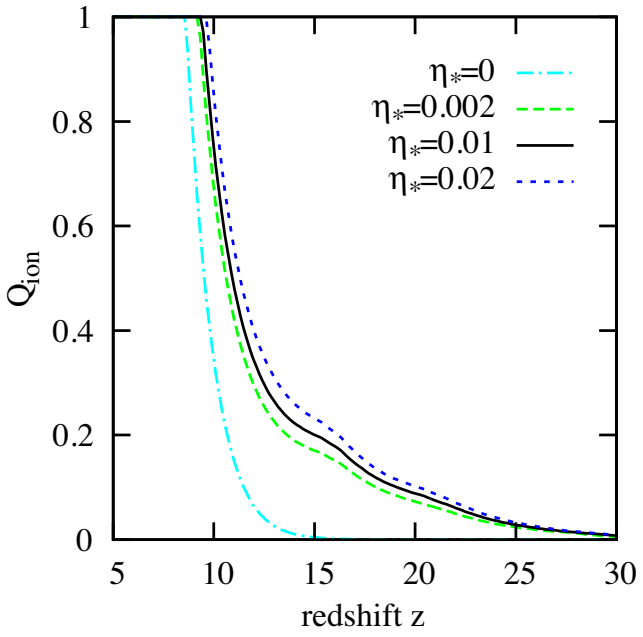

Figure 14. Volume filling fraction of the ionized IGM as a function of redshift. Values for the standard case ($f_{\mathrm{esc,\,III}} = 0.7$ and $f_{\mathrm{esc}} = 0.3$), whereas $\eta_* = 0$ represents the Pop I/II-only model for comparison. In all models, reionization occurs between $z = 8$ and 10.

By modelling the history of Pop III star formation self-consistently, we are also able to determine the most important feedback mechanisms and related quantities. For most of the time, the critical mass threshold for H_2 cooling is the dominant suppression mechanism for primordial star formation and only at smaller redshifts the radiative and chemical feedback becomes important. We find that the Pop III star formation rate peaks at $z \sim 20$ and that each successfully Pop III-forming halo has an average stellar mass content of $\sim 100\,\mathrm{M}_\odot$. However, this stellar mass content per halo has a huge scatter between 25 and $500\,\mathrm{M}_\odot$, reflecting the stochastic nature of star formation. Also the multiplicity of Pop III systems shows a large scatter with a clear trend to systems with multiple stars.

The presented model and statistical analysis is based on several assumptions and simplifications. However, we have shown that the conclusions are very robust with respect to changes in

fundamental model parameters. Moreover, most assumptions in our model tend to underestimate the number of Pop III survivors and therefore even strengthen our final conclusion. This model can be improved by including the proper spatial distribution of the haloes, or a self-consistent transition from Pop III to subsequent star formation modes. The current statistical model assumes that all stars have the same observability and that they are selected randomly. To improve this model, one could think of a weighting function, taking into account different degrees of observability together with selection criteria for follow-up spectroscopic surveys.

In future work, we will compare our analytical model to three-dimensional simulations to obtain better estimates for the spatial distribution, which is important for a proper feedback model at higher redshifts, for the planning of further surveys in the present-day halo. Moreover, a similar study with the focus on satellite galaxies and ultrafaint dwarfs could reveal interesting additional results and better constraints, in order to provide a well-considered observation plan for upcoming surveys.

Besides a fundamental insight in the primordial SFH and an estimation for the low-mass end of the Pop III IMF, we also provide a target sample size for upcoming surveys. Hitherto, the prime target of stellar archaeology was to identify individual intriguing, record-setting EMP stars; now, we are entering a novel phase of discovery, where statistically representative samples with well-controlled selection and incompleteness biases will become key goals. Put differently: even the absence of record-setting stars provides powerful constraints, provided that the underlying surveys are fairly sampling the metal-poor tail of the Galactic stellar system.

ACKNOWLEDGEMENTS

TH thanks Jeremy Ritter for his hospitality and fruitful discussions during the stay in Austin. Moreover, we would like to thank Marta Volonteri, Ken Freeman, Norbert Christlieb, Paul Clark, Mei Sasaki, Anna Frebel, Brendan Griffen, Greg Dooley, Alex Ji, and the anonymous referee for helpful comments and contributions. TH, RSK, and SCOG are supported from the European Research Council under the European Community's Seventh Framework Programme (FP7/2007-2013) via the ERC Advanced Grant 'STARLIGHT: Formation of the First Stars' (project number 339177). The simulations described in this paper were performed on the *kolob* cluster at the University of Heidelberg, which is funded in part by the DFG via Emmy-Noether grant BA 3706, and via a Frontier grant of Heidelberg University, sponsored by the German Excellence Initiative as well as the Baden-Württemberg Foundation. Moreover, TH acknowledges funding from the European Research Council under the European Community's Seventh Framework Programme (FP7/2007-2013 Grant agreement no. 614199, project 'BLACK'). VB acknowledges support from NSF grants AST-1009928 and AST-1413501. SCOG acknowledges support from the DFG via SFB 881, 'The Milky Way System' (subprojects B1, B2 and B8). The authors have employed the publicly available GALFORM and CAMB codes.

REFERENCES

Abel T., Bryan G. L., Norman M. L., 2002, Science, 295, 93
Alvarez M. A., Wise J. H., Abel T., 2009, ApJ, 701, L133
Aoki W., Tominaga N., Beers T. C., Honda S., Lee Y. S., 2014, Science, 345, 912
Barkana R., Loeb A., 2007, Rep. Prog. Phys., 70, 627
Beers T. C., Christlieb N., 2005, ARA&A, 43, 531
Bland-Hawthorn J., Maloney P. R., 1999, ApJ, 510, L33
Bland-Hawthorn J., Peebles P. J. E., 2006, Science, 313, 311
Bland-Hawthorn J., Krumholz M. R., Freeman K., 2010, ApJ, 713, 166
Blum R. D., 1995, ApJ, 444, L89
Bond J. R., Cole S., Efstathiou G., Kaiser N., 1991, ApJ, 379, 440
Bromm V., 2013, Rep. Prog. Phys., 76, 112901
Bromm V., Coppi P. S., Larson R. B., 2002, ApJ, 564, 23
Brook C. B., Kawata D., Scannapieco E., Martel H., Gibson B. K., 2007, ApJ, 661, 10
Caffau E. et al., 2011, Nature, 477, 67
Caffau E. et al., 2013, A&A, 560, A71
Campisi M. A., Maio U., Salvaterra R., Ciardi B., 2011, MNRAS, 416, 2760
Christlieb N., Schörck T., Frebel A., Beers T. C., Wisotzki L., Reimers D., 2008, A&A, 484, 721
Clark P. C., Glover S. C. O., Smith R. J., Greif T. H., Klessen R. S., Bromm V., 2011a, Science, 331, 1040
Clark P. C., Glover S. C. O., Klessen R. S., Bromm V., 2011b, ApJ, 727, 110
Cole S., Lacey C. G., Baugh C. M., Frenk C. S., 2000, MNRAS, 319, 168
de Bennassuti M., Schneider R., Valiante R., Salvadori S., 2014, MNRAS, 445, 3039
Diemand J., Madau P., Moore B., 2005, MNRAS, 364, 367
Dopcke G., Glover S. C. O., Clark P. C., Klessen R. S., 2013, ApJ, 766, 103
Draine B. T., 2011, Physics of the Interstellar and Intergalactic Medium. Princeton Univ. Press, Princeton
Ekström S., Meynet G., Chiappini C., Hirschi R., Maeder A., 2008, A&A, 489, 685
Frebel A., 2010, Astron. Nachr., 331, 474
Frebel A., Johnson J. L., Bromm V., 2009, MNRAS, 392, L50
Freeman K., Bland-Hawthorn J., 2002, ARA&A, 40, 487
Freese K., Bodenheimer P., Spolyar D., Gondolo P., 2008, ApJ, 685, L101
Friel E. D. et al., 2014, A&A, 563, A117
García Pérez A. E. et al., 2013, ApJ, 767, L9
Glover S., 2013, in Wiklind T., Mobasher B., Bromm V., eds, Astrophysics and Space Science Library, Vol. 396, The First Stars. Springer-Verlag, Berlin, p. 103
Glover S. C. O., Brand P. W. J. L., 2003, MNRAS, 340, 210
Greif T. H., 2014, preprint (arXiv:1410.3482)
Greif T. H., Bromm V., 2006, MNRAS, 373, 128
Greif T. H., White S. D. M., Klessen R. S., Springel V., 2011a, ApJ, 736, 147
Greif T. H., Springel V., White S. D. M., Glover S. C. O., Clark P. C., Smith R. J., Klessen R. S., Bromm V., 2011b, ApJ, 737, 75
Greif T. H., Bromm V., Clark P. C., Glover S. C. O., Smith R. J., Klessen R. S., Yoshida N., Springel V., 2012, MNRAS, 424, 399
Haiman Z., Thoul A. A., Loeb A., 1996a, ApJ, 464, 523
Haiman Z., Rees M. J., Loeb A., 1996b, ApJ, 467, 522
Haiman Z., Abel T., Rees M. J., 2000, ApJ, 534, 11
Hartwig T., Clark P. C., Glover S. C. O., Klessen R. S., Sasaki M., 2014, preprint (arXiv:1407.2102)
Heger A., Woosley S. E., 2002, ApJ, 567, 532
Heger A., Woosley S. E., 2010, ApJ, 724, 341
Hirano S., Hosokawa T., Yoshida N., Umeda H., Omukai K., Chiaki G., Yorke H. W., 2014, ApJ, 781, 60
Hopkins A. M., Beacom J. F., 2006, ApJ, 651, 142
Hosokawa T., Yoshida N., Omukai K., Yorke H. W., 2012, ApJ, 760, L37
Iocco F., 2008, ApJ, 677, L1
Islam R. R., Taylor J. E., Silk J., 2003, MNRAS, 340, 647
Islam R. R., Taylor J. E., Silk J., 2004a, MNRAS, 354, 427
Islam R. R., Taylor J. E., Silk J., 2004b, MNRAS, 354, 443
Jeon M., Pawlik A. H., Bromm V., Milosavljević M., 2014, MNRAS, 440, 3778
Jiang F., van den Bosch F. C., 2014, MNRAS, 440, 193
Johnson J. L., 2014, preprint (arXiv:1411.4189)
Johnson J. L., Bromm V., 2006, MNRAS, 366, 247
Johnson J. L., Greif T. H., Bromm V., 2008, MNRAS, 388, 26
Karlsson T., Johnson J. L., Bromm V., 2008, ApJ, 679, 6
Karlsson T., Bromm V., Bland-Hawthorn J., 2013, Rev. Mod. Phys., 85, 809

Keller S. C. et al., 2014, Nature, 506, 463
Kitayama T., Yoshida N., Susa H., Umemura M., 2004, ApJ, 613, 631
Kroupa P., 2001, MNRAS, 322, 231
Kulkarni G., Rollinde E., Hennawi J. F., Vangioni E., 2013, ApJ, 772, 93
Kulkarni G., Hennawi J. F., Rollinde E., Vangioni E., 2014, ApJ, 787, 64
Lacey C., Cole S., 1993, MNRAS, 262, 627
Lewis A., Challinor A., Lasenby A., 2000, ApJ, 538, 473
Li L.-X., 2008, MNRAS, 388, 1487
Loeb A., 2010, How Did the First Stars and Galaxies Form? Princeton Univ. Press, Princeton
Loeb A., Furlanetto S. R., 2013, The First Galaxies in the Universe. Princeton Univ. Press, Princeton
Machacek M. E., Bryan G. L., Abel T., 2001, ApJ, 548, 509
Machacek M. E., Bryan G. L., Abel T., 2003, MNRAS, 338, 273
McMillan P. J., 2011, MNRAS, 414, 2446
Madau P., Dickinson M., 2014, ARA&A, 52, 415
Maio U., Koopmans L. V. E., Ciardi B., 2011, MNRAS, 412, L40
Mapelli M., Ferrara A., Rea N., 2006, MNRAS, 368, 1340
Marigo P., Girardi L., Chiosi C., Wood P. R., 2001, A&A, 371, 152
Mesler R. A., Whalen D. J., Smidt J., Fryer C. L., Lloyd-Ronning N. M., Pihlström Y. M., 2014, ApJ, 787, 91
Mirabel I. F., Dijkstra M., Laurent P., Loeb A., Pritchard J. R., 2011, A&A, 528, A149
Moretti A., Vattakunnel S., Tozzi P., Salvaterra R., Severgnini P., Fugazza D., Haardt F., Gilli R., 2012, A&A, 548, A87
Nakamura F., Umemura M., 2002, ApJ, 569, 549
Ness M. et al., 2013, MNRAS, 430, 836
O'Shea B. W., Norman M. L., 2008, ApJ, 673, 14
Oh S. P., 2001, ApJ, 553, 499
Omukai K., Palla F., 2001, ApJ, 561, L55
Omukai K., Palla F., 2003, ApJ, 589, 677
Paardekooper J.-P., Khochfar S., Dalla Vecchia C., 2013, MNRAS, 429, L94
Pallottini A., Ferrara A., Gallerani S., Salvadori S., D'Odorico V., 2014, MNRAS, 440, 2498
Parkinson H., Cole S., Helly J., 2008, MNRAS, 383, 557
Planck Collaboration XVI, 2014, A&A, 571, 16
Power C., Wynn G. A., Combet C., Wilkinson M. I., 2009, MNRAS, 395, 1146
Press W. H., Schechter P., 1974, ApJ, 187, 425
Rafelski M., Wolfe A. M., Prochaska J. X., Neeleman M., Mendez A. J., 2012, ApJ, 755, 89
Rees M. J., 1976, MNRAS, 176, 483
Ritter J. S., Sluder A., Safranek-Shrader C., Milosavljevic M., Bromm V., 2014, preprint (arXiv:1408.0319)
Robertson B. E. et al., 2013, ApJ, 768, 71
Salpeter E. E., 1955, ApJ, 121, 161
Salvadori S., Ferrara A., 2012, MNRAS, 421, L29
Salvadori S., Schneider R., Ferrara A., 2007, MNRAS, 381, 647
Salvadori S., Ferrara A., Schneider R., Scannapieco E., Kawata D., 2010, MNRAS, 401, L5
Salvadori S., Tolstoy E., Ferrara A., Zaroubi S., 2014, MNRAS, 421, L29
Salvaterra R., Haardt F., Volonteri M., Moretti A., 2012, A&A, 545, L6
Sasaki M., Clark P. C., Springel V., Klessen R. S., Glover S. C. O., 2014, MNRAS, 442, 1942
Scannapieco E., Kawata D., Brook C. B., Schneider R., Ferrara A., Gibson B. K., 2006, ApJ, 653, 285
Schaerer D., 2002, A&A, 382, 28
Schleicher D. R. G., Banerjee R., Klessen R. S., 2008, Phys. Rev. D, 78, 083005
Schleicher D. R. G., Glover S. C. O., Banerjee R., Klessen R. S., 2009a, Phys. Rev. D, 79, 023515
Schleicher D. R. G., Banerjee R., Klessen R. S., 2009b, Phys. Rev. D, 79, 043510
Schleicher D. R. G., Banerjee R., Sur S., Arshakian T. G., Klessen R. S., Beck R., Spaans M., 2010, A&A, 522, A115
Schober J., Schleicher D. R. G., Federrath C., Glover S. C. O., Klessen R. S., Banerjee R., 2012, ApJ, 754, 99
Sedov L. I., 1959, Similarity and Dimensional Methods in Mechanics. Academic Press, New York
Smith R. J., Iocco F., Glover S. C. O., Schleicher D. R. G. Klessen R. S., Hirano S., Yoshida N., 2012, ApJ, 761, 154
Spolyar D., Bodenheimer P., Freese K., Gondolo P., 2009, ApJ, 705, 1031
Springel V. et al., 2005, Nature, 435, 629
Stacy A., Bromm V., 2014, ApJ, 785, 73
Stacy A., Greif T. H., Bromm V., 2010, MNRAS, 403, 45
Stacy A., Bromm V., Loeb A., 2011, ApJ, 730, L1
Stacy A., Greif T. H., Bromm V., 2012, MNRAS, 422, 290
Stacy A., Greif T. H., Klessen R. S., Bromm V., Loeb A., 2013, MNRAS, 431, 1470
Sur S., Schleicher D. R. G., Banerjee R., Federrath C., Klessen R. S., 2010, ApJ, 721, L134
Taylor G., 1950, Proc. R. Soc. A, 201, 159
Trenti M., Stiavelli M., 2009, ApJ, 694, 879
Tseliakhovich D., Hirata C., 2010, Phys. Rev. D, 82, 083520
Tseliakhovich D., Barkana R., Hirata C. M., 2011, MNRAS, 418, 906
Tumlinson J., 2006, ApJ, 641, 1
Tumlinson J., 2010a, ApJ, 708, 1398
Tumlinson J., 2010b, in Whalen D. J., Bromm V., Yoshida N., eds, AIP Conf. Ser. Vol. 1294, The First and Second Stars: How to Find Them and What to Do About It (or, Three Big Ideas and Three Challenges). Am. Inst. Phys., New York, p. 84
Volonteri M., 2012, Science, 337, 544
Volonteri M., Bellovary J., 2012, Rep. Prog. Phys., 75, 124901
White S. D. M., Rees M. J., 1978, MNRAS, 183, 341
White S. D. M., Springel V., 2000, in Weiss A., Abel T. G., Hill V., eds, The First Stars Where Are the First Stars Now? Springer-Verlag, Berlin, p. 327
Widrow L. M., Dubinski J., 2005, ApJ, 631, 838
Wise J. H., Abel T., 2007, ApJ, 671, 1559
Yoshida N., Abel T., Hernquist L., Sugiyama N., 2003, ApJ, 592, 645
Yoshida N., Omukai K., Hernquist L., 2007, ApJ, 667, L117

This paper has been typeset from a TEX/LATEX file prepared by the author.